MICROFLUIDIC SYSTEM WITH OPEN LOOP CONTROL FOR RAPID INFRARED REVERSE TRANSCRIPTION QUANTITATIVE PCR (RT-QPCR)

A Thesis
Presented to
The Academic Faculty

by

Daniel Curtis Saunders

In Partial Fulfillment
of the Requirements for the Degree
Master of Science in the
School of Mechanical Engineering

Georgia Institute of Technology
August 2012

MICROFLUIDIC SYSTEM WITH OPEN LOOP CONTROL FOR RAPID INFRARED REVERSE TRANSCRIPTION QUANTITATIVE PCR (RT-QPCR)

Approved by:

Dr. Craig Forest, Advisor
School of Mechanical Engineering
Georgia Institute of Technology

Dr. Samuel Graham
School of Mechanical Engineering
Georgia Institute of Technology

Dr. Todd Sulchek
School of Mechanical Engineering
Georgia Institute of Technology

Date Approved: June 25, 2012

ACKNOWLEDGEMENTS

There are many people I wish to thank for helping me with this project. First and foremost I would like to thank my advisor, Prof. Craig Forest. Craig's knowledge and guidance with this project has been instrumental in its development and success. Furthermore his enthusiasm and support for his students and his dedication to cultivating an innovative and collaborative atmosphere in lab is remarkable. I would also like to thank my other committee members, Profs. Samuel Graham and Todd Sulchek for agreeing to be on my Master's committee, for meeting with me to discuss the project, and for their feedback on the work.

In addition I would like to thank my fellow members of the Precision Biosystems Lab. I would like to thank Chris for his help with assembling and testing various components in the laser system, for teaching me all the PCR reaction preparation techniques I know, and thanks to both Chris and Nick for supplying me with limitless quantities of 'chris chips'. I would like to thank Greg for his help with the chip pressurization assembly, environmental chamber design, and optimized power profile work as well as for being a sounding board for various problems and fixes. Thanks also to Mel for helping me with the statistical analysis of the data, and to Nikita for helping me with the Labview programs and for running my PCR samples on the Bioanalyzer whenever I was running short on time.

Finally, I would like to thank my friends and family. Their love and support are invaluable and I will always be deeply grateful.

TABLE OF CONTENTS

LIST OF FIGURES

SUMMARY

Microfluidic techniques have allowed for fast, sensitive, and low cost applications of the Polymerase Chain Reaction (PCR) through the use of small reaction volumes, rapid amplification speeds, and the on-chip integration of upstream and downstream sample handling processes including purification and electrophoretic separation functionality. While such systems are capable of measuring the expression levels of thousands of genes simultaneously, or in hundreds of cells, or with sample-in and answer-out capability, none of these systems are easily scalable in the time domain. Because of this, the field of gene expression measurement has yet to fully utilize the advantages of microfluidic PCR in developing systems to measure changes in gene expression in increments of hours rather than days. In this project, we developed a microfluidic RT-qPCR system that utilizes infrared heating and open-loop control to reliably reverse transcribe, amplify, and detect samples in a single 1 μl polymer chip. Optimized power profiles were created that allow for fast heating and cooling rates while minimizing undershoot and overshoot from the desired hold temperatures. By utilizing repeatable microfluidic chip manufacturing techniques, and by controlling the environment around the chip, the same open loop program can repeatedly amplify multiple samples without any need for temperature feedback or recalibration between runs. Furthermore, the system was designed to operate on top of a fluorescence microscope to enable real-time fluorescence detection and quantification of starting copy number. By eliminating complicated setup procedures and calibration runs, this system increases the practicality of measuring gene expression at a high temporal frequency.

CHAPTER 1

INTRODUCTION

Overview of PCR

The Polymerase Chain Reaction is a DNA amplification technique developed by Kary Mullis and colleagues in 1983 [1]. It is a temperature-controlled and enzyme-catalyzed biochemical reaction that consists of the repeated cycling through three distinct temperatures, denaturation, annealing, and extension. The reaction consists of a DNA template, two oglionucletide primers that are complementary to the ends of the DNA sequence to be amplified, dNTP's, a heat stable polymerase, and magnesium ions in a reaction buffer [2]. The reaction is first heated to 93 °C, the denaturation temperature, at which point the double stranded DNA separates into two single strands. The reaction is then cooled to allow the primers to anneal to the specific sequences of target DNA, usually 50 – 68 °C, depending on the length and sequence of primers. Finally, the reaction is heated to 72 ° C, the optimum temperature for the Taq polymerase to fully extend the primer sequences by incorporating the dNTP's into the strands of DNA, effectively doubling the amount of DNA in the reaction (Figure 1).

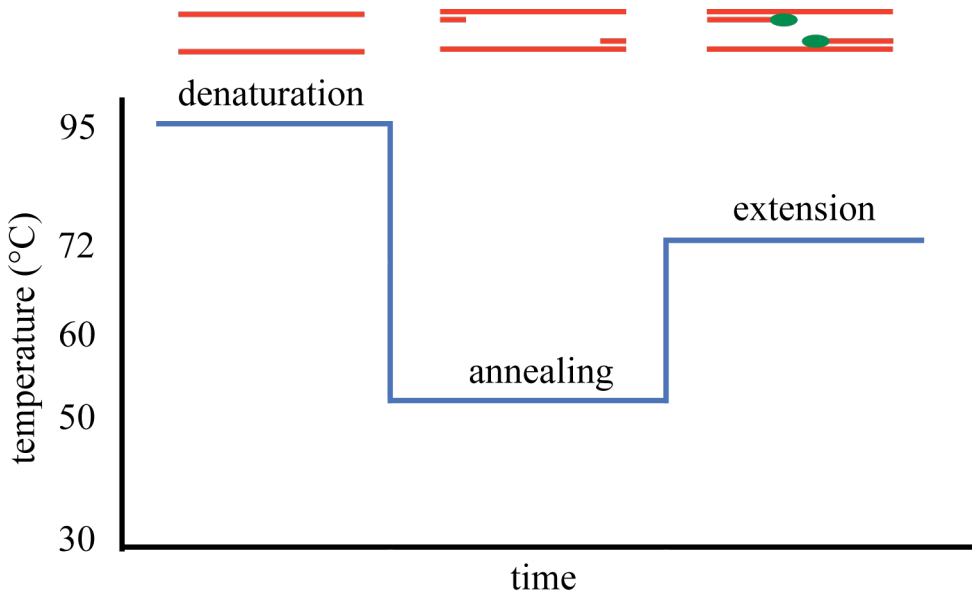

Figure 1: The three temperatures in the PCR cycle: denaturation, annealing, and extension. At denaturation, the double stranded DNA melts and separates into two single strands. During annealing, primers complimentary to the target segment of DNA attach to the strands and during extension, the Taq polymerase extends the segments by incorporating the extra dNTP's into the strand (reproduced from [2]).

The temperature cycle repeats and the reaction continues until the primers, dNTP's or Taq Polymerase is depleted, at which point the concentration of DNA template plateaus. Effectively doubling the amount of target DNA after each cycle means that tens or hundreds of starting copies can generate millions of copies of a specific DNA sequence after only 30 – 40 cycles. Since its introduction almost 30 years ago, the PCR process has been applied to a wide variety of fields, from biomedical research laboratories to life science areas including clinical diagnoses, as well as medical, biological, and forensic analyses [3].

Devices on the Market Today

Conventional PCR machines on the market today usually consist of a large metal block and Peltier Thermo-Electric element for the thermal cycling, a closed-loop feedback system, and a user interface and control module for setting cycle hold times and temperatures [4]. The heating method used by these devices is generally referred to as

contact heating, in which the Thermo-Electric element heats and cools a metal block surrounding the sample, which in turn heats and cools the sample. These devices use relatively large sample volumes (25 – 50 µl) and relatively long run times (1 – 2 hrs) [5, 6]. Due to the relatively low surface area to volume ratio of the sample and high thermal mass of the system, heating and cooling rates are slow (1 – 2 °C/s) and often non-specific PCR products are formed during the transition temperatures, decreasing the efficiency and specificity of the reaction. Alternatives to conventional thermocyclers include the Roche Lightcycler [7] and Qiagen Rotor Gene Q that use convective heating and fluorescence detection for real-time PCR with volumes as low as several microliters. Though effective, their cost and complexity limit scalability, speed, compatibility with field deployment, and volume reduction.

Sample Detection Methods

End Point Detection

The two common techniques to quantify PCR product are end point detection and real-time detection. End point detection quantifies the amount of PCR product amplified after the reaction is completed. At this point in the reaction, the limiting reagent has been depleted and the concentration of DNA template has plateaued. The PCR product is measured by either adding an intercalating dye that binds to only double-stranded DNA and measuring the increase in fluorescence intensity of the sample after the completion of the reaction or by post-processing the sample via off-line detection techniques such as capillary or gel electrophoresis [8]. Because the limiting reagent and reaction efficiency can vary from sample to sample, based on reagent limitation or accumulation of non-specific PCR products, the plateau phase of the reaction is highly variable and end point detection is not a reliable way to quantify starting copies of a DNA template [9].

Exponential Phase Detection

Exponential phase detection, or quantitative PCR (qPCR) quantifies the amount of PCR product formed during the exponential phase of the reaction. Generally, an intercalating dye that binds to only double-stranded DNA or fluorescent probe complimentary to the DNA target of interest is added to the reaction (Figure 2).

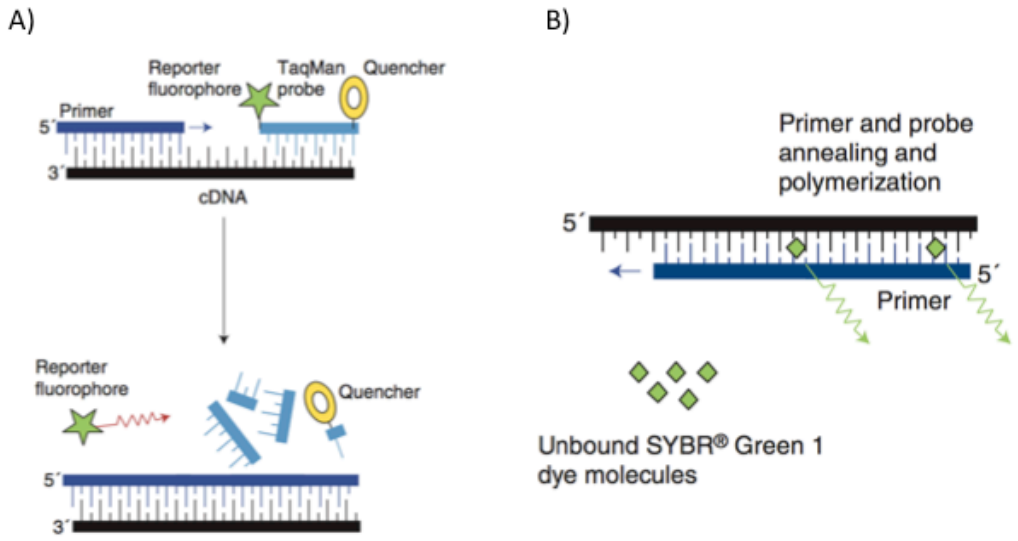

Figure 2: Fluorescence for Real-Time PCR is measured with either A) a fluorescent probe complimentary to the DNA target of interest or with B) an intercalating dye that only binds to double-stranded DNA (reproduced from [9]).

As the amount of DNA increases, the fluorescence intensity of the sample increases. After the first 5 – 15 PCR cycles, the fluorescence intensity reaches the detection limit of the system and begins to exponentially increase. It continues to increases exponentially until the limiting reagent in the reaction is depleted, at which point the fluorescence intensity plateaus. By determining the number of cycles the reaction completes before crossing the detection threshold (CT value), one can determine the starting concentration of DNA template (Figure 3).

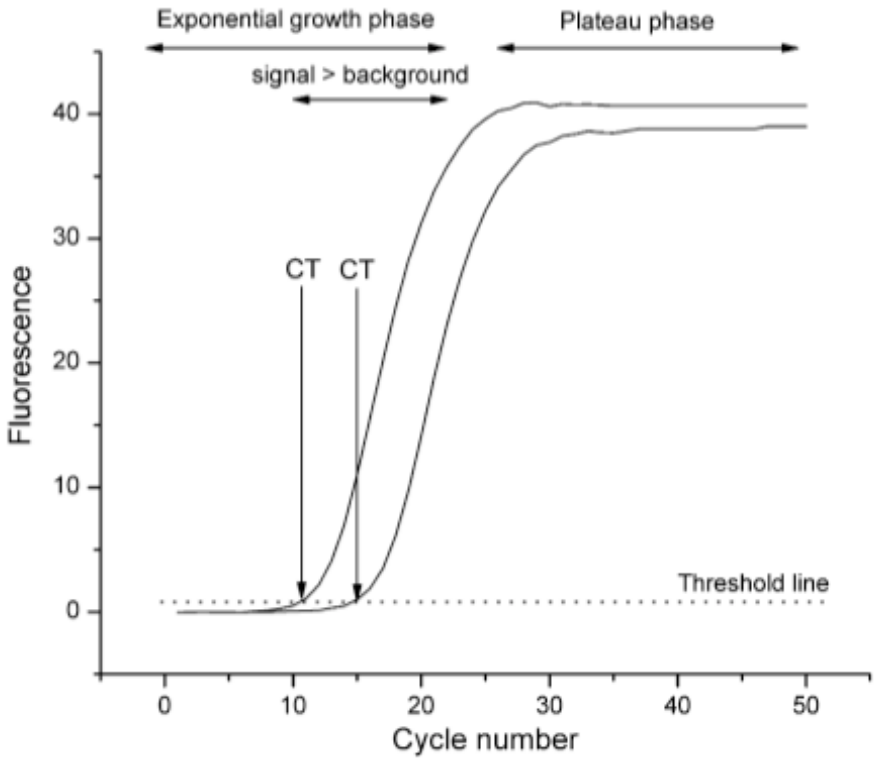

Figure 3: Real-Time PCR graph showing sample fluorescence as a function of temperature cycles for two samples with different starting concentrations of DNA template. The cycle number at which the fluorescence signal begins to exponentially increase is directly proportional to the starting concentration of DNA template and is referred to as the CT value for the reaction (reproduced from [2]).

Because this technique monitors the reaction during the exponential phase and no limiting reagent has been depleted, the technique is more repeatable and DNA template starting concentration can be determined accurately [9]. The increased resolution and accuracy of exponential phase detection techniques makes it the preferred method when knowing the starting concentration of the template is critical. However, when only testing for the presence and not necessarily concentration of a certain DNA template, such as in virus detection or disease diagnostics, conventional end-point detection techniques are still used.

Gene Expression Measurement

Quantitative PCR (qPCR) is currently used for a wide range of applications including mRNA expression studies, viral or genomic DNA copy number measurements, allelic discrimination assays, expression analysis of specific splice variants of genes, gene expression in paraffin-embedded tissues, and laser captured microdissected cells [9]. For studies involving RNA quantification, a modified version of qPCR, reverse transcription quantitative PCR (RT-qPCR), is used to quantify the amounts of specific sequences of RNA being produced by cells. These unique sequences of RNA in the cell are defined as genes, so the number of copies of a certain sequence of RNA in either a cell or a population of cells is referred to as the expression level of that gene.

To perform qPCR on RNA, the *single-stranded* RNA of the sample must first be reverse-transcribed into *double-stranded* DNA. To accomplish this, often both primers and a reverse transcriptase are added to the RNA sample and held at a constant temperature for 0.5 – 1 hrs. The primers attach to sections of the RNA, creating sites for the reverse transcriptase to begin transcribing the single stranded RNA into complementary double stranded DNA (cDNA) [2]. A complete reverse-transcription step where all RNA is transcribed into cDNA is necessary to ensure accurate quantification of the amount of RNA in the sample. This process is generally accomplished using large bench-top thermal cyclers, with comparable sample volumes to conventional PCR (25 – 50 μl), but with run times ranging from 2.5 – 4 hrs.

Quantification Methods

The expression level of a gene in a reaction can be determined absolutely or relative to another gene in the reaction. In absolute quantification, the exact number of copies of a specific gene in a sample is determined. It was first shown by Higuchi et al. that for quantitative PCR, the plot of the log of starting copy number for a series of serial dilutions versus the cycle threshold values is a straight line [10]. Therefore, to determine

the starting copy number of a sample, a set of dilutions with known copy numbers of the same target of interest is run in parallel with the sample(s) and the starting copy number of the unknown sample is determined by comparing the cycle threshold number of the sample of unknown concentration to those of the known dilutions, or standards. This is referred to as the standard curve (Figure 4).

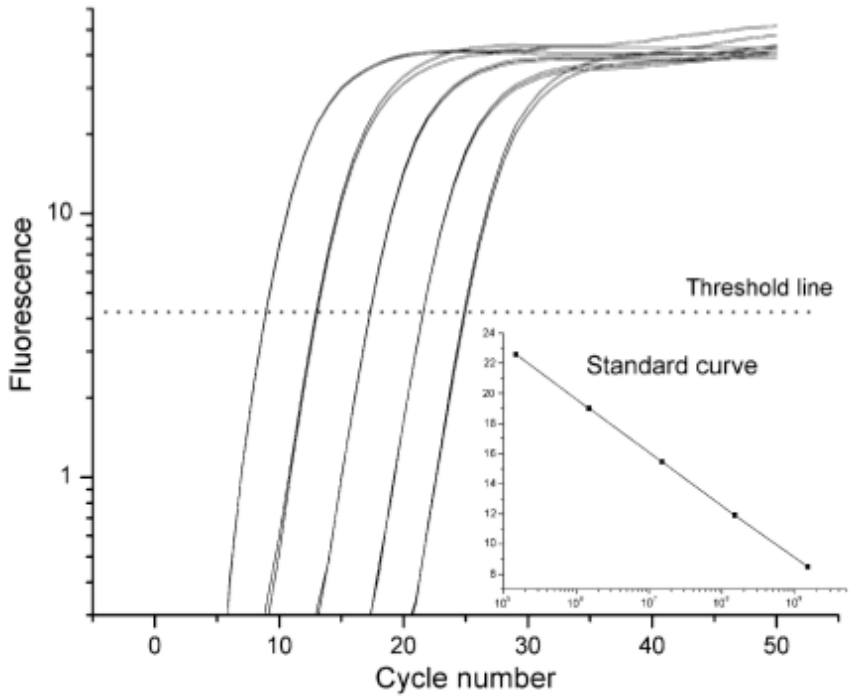

Figure 4: Quantitative PCR plot showing sample fluorescence as a function of cycle number for a series of 5 – 10x dilutions of a DNA template with known starting copy numbers. The subset plot shows the cycle threshold values (CT) as a function of the log of the starting copy number for the 5-10x dilutions. This relationship is known to be a straight line (reproduced from [2]).

Relative quantification compares the normalized cycle threshold values (CT) between two genes of interest. Biological samples are often heterogeneous and the amount of biological material present in samples can vary significantly. Therefore, comparing absolute levels of gene expression between two samples would be unreliable. Instead, the expression levels of two genes are calculated relative to a control gene or housekeeping gene whose expression is known to remain constant for different experimental conditions. The relative expression level is defined as,

$$\frac{Sample1}{Sample2} = \frac{2^{CT_{B1}-CT_{B2}}}{2^{CT_{A1}-CT_{A2}}} = 2^{(CT_{B1}-CT_{B2})-(CT_{A1}-CT_{A2})} \quad \textbf{(Eq. 1)}$$

where CT_{A1} and CT_{B1} are the cycle threshold values for the genes of interest and CT_{A2} and CT_{B2} are the cycle threshold values for the housekeeping gene.

This method of relative quantification is often referred to as the $2^{-\Delta\Delta Ct}$ method [9].

Other Gene Expression Measurement Techniques

In addition to RT-qPCR, other methods of measuring the transcriptional levels of RNA in cells and tissues include fluorescence-activated cell sorting (FACS), fluorescence *in situ* hybridization (FISH), microarrays, and RNA sequencing [11, 12]. In FACS, a fluorescence-activated cell sorter is used to separate certain fluorescently tagged cells from a heterogeneous cell population. Since the heterogeneity of cell populations can vary, FACS is often used to purify cells expressing a certain gene from populations before RT-qPCR analysis which is often used after FACS for more accurate quantification of gene expression levels within the sorted cell population [11].

While FACS is an efficient way to isolate a cell population, the technique does not preserve the spatial context of gene expression in tissues or cell cultures. Fluorescence *in situ* hybridization (FISH) is commonly used when knowledge about the spatial distribution of gene expressions in cells or tissues is necessary. Typically, a probe with a fluorescently labeled transcript or nucleotide of interest is added to permeabilized cells or tissues. If the gene or nucleotide of interest is present in the sample, the probe will hybridize to the gene and will fluoresce when the sample is imaged [11]. Recent improvements in imaging technology and processing software as well as improved probe designs have significantly increased the spatial localization of signals, enabling single-molecule transcript imaging [11]. However, scalability of this technology to multiple genes in multiple cells and tissues is hindered by expensive equipment, and the need for long recording times and high-intensity illumination [11].

Unlike FACS and FISH, microarray and RNA sequencing technologies are easily scalable for high-throughput quantification of multiple RNA targets of interest. Microarrays for measuring gene expression were first developed in 1995 by Schena et al. and have since become widely used in profiling the gene expression of cells [13]. Microarrays typically consist of an array containing hundreds to thousands of wells that each contains a set of short oglionucleotide probes representing segments of DNA. RNA is purified from cells, reverse-transcribed into cDNA, labeled with a fluorescent dye and then washed over the microarray. Probes that correspond to the transcribed RNA will hybridize to the complementary target. After hybridization and washing, the array is imaged and since the transcripts are labeled with fluorescent dyes, fluorescence intensity in different wells can be used as a measure of gene expression [12]. This method allows researchers to quickly test for expression levels of hundreds to hundreds of thousands of genes. However, due to the reduced sensitivity of microarrays, they are primarily used to quickly identify genes of interest to be further screened via conventional RT-qPCR [14].

In contrast to microarrays where the specific targets of interest need to be know ahead of time, RNA sequencing technologies can be used to map a sample with no prior knowledge of the sample's genome structure [12]. This technology directly maps the genes present in the sample and the number of mapped reads of a particular sequence enables a measure of the expression level of that particular gene.

Gene Expression in Stem Cells

One emerging area for increased RNA expression studies is the field of functional genomics and specifically gene expression in stem cells [15]. Stem cells are cells that have the ability to self-renew as well as differentiate into other cell types. Stem cells are classified as either totipotent, pluirpotent, multipotent, or unipotent, based on their differentiation capability [16]. Stem cells have broad applications in engineering and regenerative medicine, from better understanding cell fate determination to growing

organs and tissues for transplant purposes. However, despite the increased knowledge about the mechanisms behind how stem cells differentiate, little is known about how the gene expression pattern governing these actions is changing [15, 17]. Although multiple techniques exist for measuring gene expression in cells, the sensitivity, specificity, and wide dynamic range of RT-qPCR make it the gold standard method for quantifying gene expression [18].

Thesis Goals

This thesis will discuss the creation of a system that represents a significant contribution towards measuring cellular gene expression levels in a high-throughput temporal manner. The following chapters detail the motivation behind such a system and why existing systems cannot easily measure gene expression in a high-throughput temporal manner, a proof of concept system, the necessary improvements in temperature control and device manufacturing, design of the resulting system, and an evaluation of the final systems performance, including temperature accuracy and stability, as well as successful reverse transcription reactions and real-time fluorescence detection resulting in the construction of a standard curve for λ phage DNA.

CHAPTER 2

MOTIVATION

Gene Expression Measurement Today

While qPCR based expression analysis remains the gold standard for quantifying gene expression changes, the high-cost of reagents and equipment, long run times and labor-intensive laboratory preparation required has caused it to remain a tool used largely to validate gene expression after differentiation has taken place, rather than monitor the gene expression changes in real-time [14]. Currently a typical comprehensive gene expression measurement study would measure gene expression in increments of 3-4 days. For a 15 day experiment, expression would be measured at days 0, 4, 7, 11, and 15. Due to normal variations in cell culturing techniques, 3 samples would be taken at each time point and the steps required include RNA purification, checking quantity and purity of the RNA, synthesizing cDNA through reverse-transcription, and running qPCR [18] (**Figure 5**).

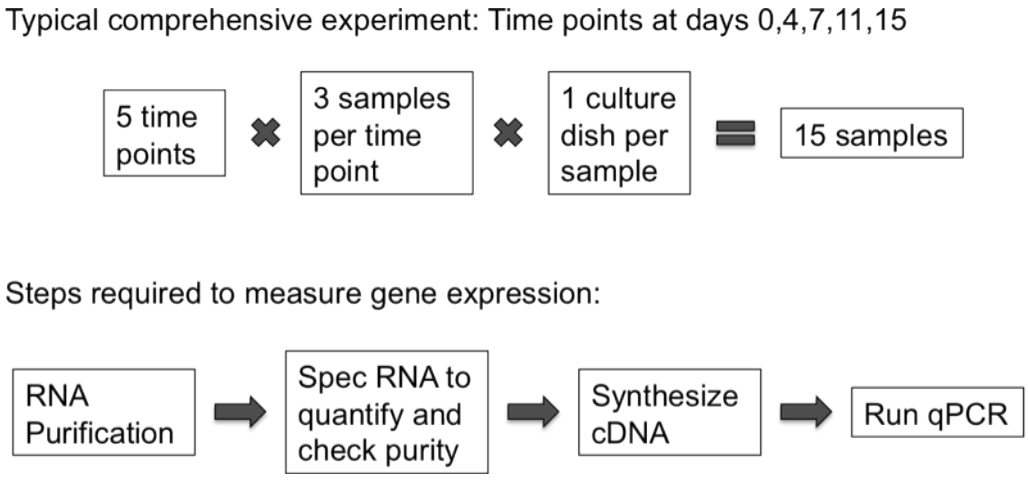

Figure 5: Typical gene expression experiment and steps necessary to quantify gene expression (obtained from [19]).

The majority of gene expression changes during cell development and differentiation generally take place over hours to days [17]. The low temporal frequency

and high cost of current measurement techniques prohibits researchers from gathering the necessary information to determine how gene expression changes and the interaction between the expression levels of genes during the differentiation process (Figure 6).

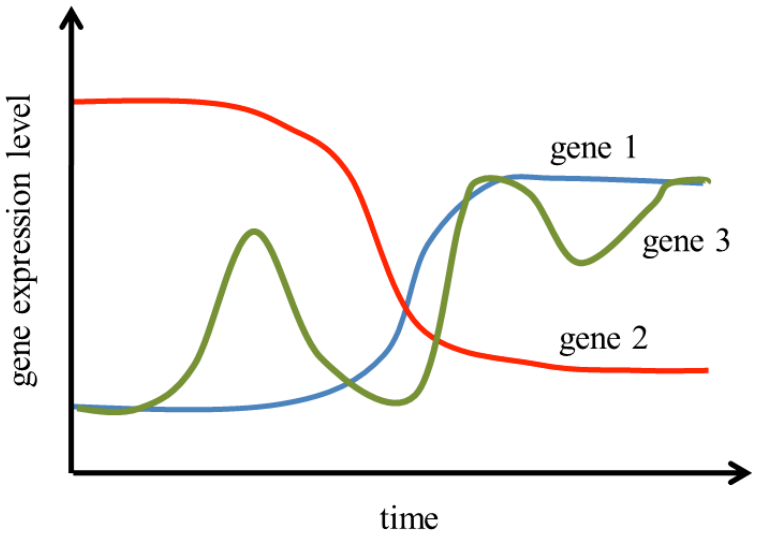

Figure 6: Illustration of the expression levels as a function of time for 3 genes of interest.

If one was to attempt to scale up the current process to measure gene expression every ½ hour for a 15 day cell differentiation experiment, it would require 864 dishes of cells, $69,519.08 spent on equipment and reagents, and take 1448 hours of labor to prepare and run the experiments (Figure 7).

Scale up experiment to measure gene expression every ½ hour for 15 days:

288 time points ✖ 3 samples per time point ✖ 1 culture dish per sample = 864 samples

Cost to run 864 samples:

Step	Extract RNA	Make cDNA	qPCR (2 genes)	Equipment	**Labor**	**Total**
Cost	$3,780.86	$3,421.44	$1,347.84	$38,500	$23,142.86	**$69,519.08**
Prep time	216 hours	40 hours	40 hours	1152 hours		**1448 hours**

Figure 7: Labor, cost, and materials required to measure gene expression every 1/2 hours for 15 days using current laboratory techniques (obtained from [19]).

The time, equipment, labor, and reagent costs required to measure gene expression quickly has prevented such work from taking place. In order to better understand the interaction between genes and how gene expression changes as a stem cell differentiates, better technology is needed for researchers.

Micro-PCR

Currently, gene expression in stem cells is measured at low spatial (population-based averaging) and temporal (every 4-6 days) frequencies due to the large sample volumes and long run times of conventional PCR instruments. However, the field of micro-PCR is enabling new research in the field of measuring gene expression. Since the first miniaturized PCR device was introduced by Northrup et al. in 1993, hundreds of microfluidic PCR chips have been developed [20]. Micro PCR technologies offer many advantages over conventional techniques. The systems have decreased fabrication costs, increased portability and integration abilities with upstream and downstream processing steps, and smaller thermal masses and diffusion distances, allowing for smaller sample volumes (1 μl), faster ramp rates (60 °C/sec) and shorter run times (under 30 min) (Figure 8) [4, 20].

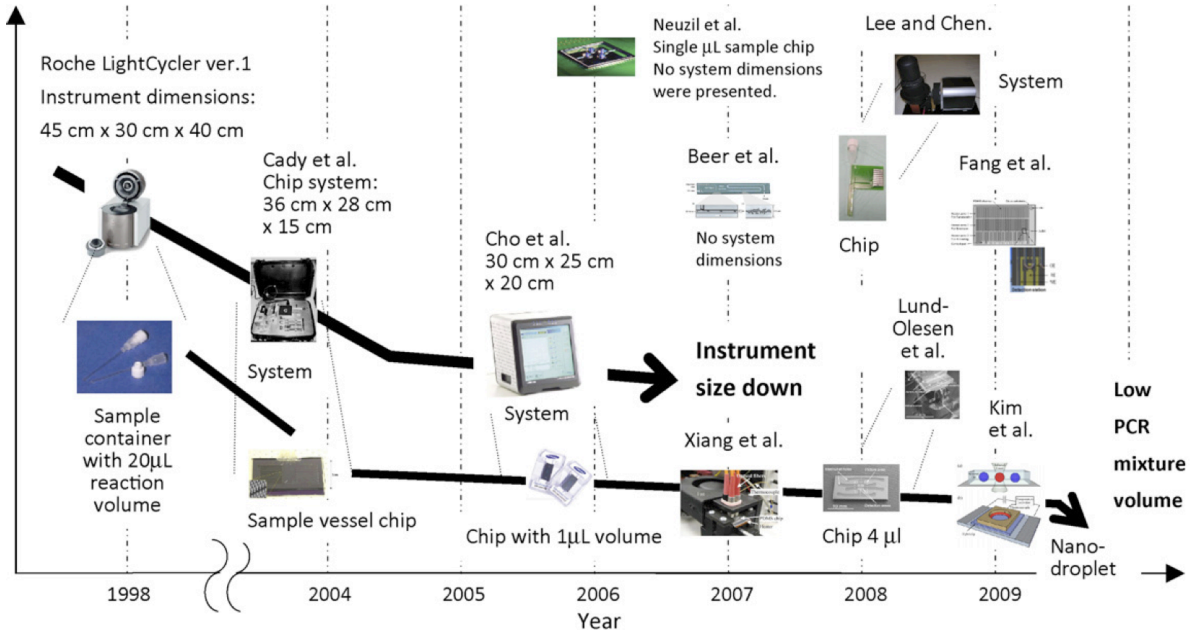

Figure 8: Since the 1990's, PCR systems have been scaling down in both reaction volume and device size [4].

Types of Devices

Micro PCR devices today can be categorized as either stationary or flow-through devices. Stationary PCR devices rely on a stationary sample and use temporal heating and cooling of the environment around the sample to cycle through the required temperatures. The sample is loaded into a chamber and is then repeatedly cycled through the denaturing, annealing, and extension temperatures (Figure 9A) [20]. PCR product quantification is also similar to conventional methods, either by post-amplification off-line detection or by measuring sample fluorescence in real-time. In contrast, for flow-through PCR, the device is divided into three different temperature zones, and these zones are simultaneously held at the denaturing, annealing, and extension temperatures specific to the reaction. To complete a temperature cycle, the reaction is moved via a channel in the chip to these three different temperature zones (Figure 9B) [20]. In these devices, PCR product quantification is often integrated into the device.

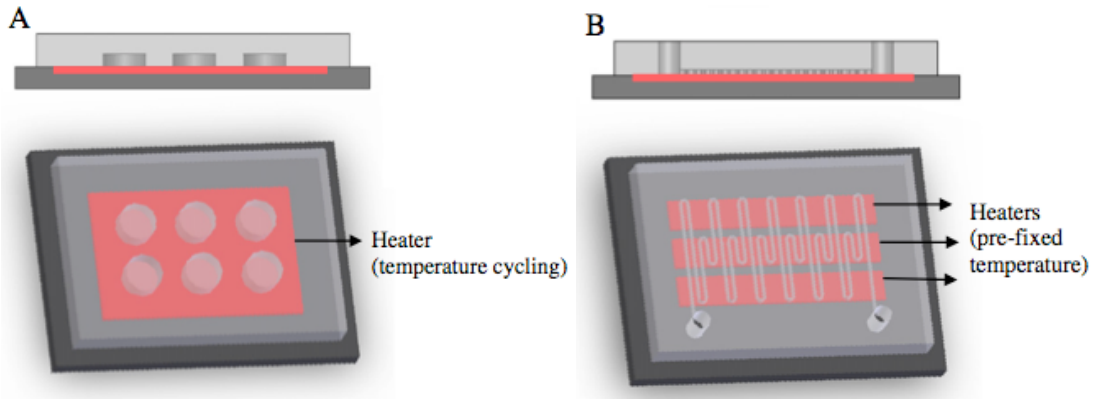

Figure 9: A) Stationary and B) Flow-through micro-PCR devices [8].

Recent work in flow-through PCR devices has focused on further decreasing the sample volume by creating droplet systems [21-23]. In these systems, discrete aqueous droplets of a fixed volume are immersed in a continuous oil phase. The droplet-oil mixture is then moved through the temperature zones. This method results in less cross-contamination between samples as well as the ability to perform high-throughput testing of many samples [8].

Heating Methods

Most micro-scale PCR devices use thermally conductive silicon or glass microchips paired with thermoelectric heating [24-27], embedded resistive heaters [28-37], or convection-based rotary platforms [7, 38-40] to offer smaller reagent volumes and faster cycling at the risk of costly fabrication and cross-contamination after multiple runs.

In contrast, direct heating via infrared radiation, pioneered by Dr. James Landers using a tungsten filament lamp [41-43] and closed-loop feedback through a thermocouple, enables rapid microliter volume thermocycling in simple, inexpensive, disposable microchips. Others have performed infrared, laser-mediated, microfluidic PCR in droplets in an oil bath after fluorescence calibration [44-46]. They were able to achieve very impressive rapid (200 s), small volume (15 pL), real-time PCR results, but the system requires a precisely aligned microscope and the small, suspended droplets

cannot be easily recovered for post-processing, making this instrument less practical for commercialization. Previous reports of calibration methods for infrared PCR have been limited by emissivity measurements with a pyrometer [42] in which accuracy is hindered by alignment and spurious reflection, or required microscopy.

Application to Gene Expression Measurement

Advances afforded by micro-PCR systems in reducing sample volume and run time, as well as integration of up-stream and down-stream processing have lead to the development of new systems to measure gene expression in cells. However, the majority of these systems have focused on either increasing the number of genes able to be simultaneously measured (e.g. microarrays), increasing the sensitivity of the system to single-cell analyses [18, 47-51], or developing systems with sample-in answer-out capabilities.

Microarrays allow for researchers to measure the expression of thousands of genes simultaneously, though usually at low spatial (population-based averaging) and temporal frequencies. This technology, along with RNA sequencing, allows for researchers to identify which genes expression changes during differentiation, and quickly and efficiently identifies targets of interest for more detailed measurement techniques. In addition, the decreased sensitivity of microarrays have meant that researchers have had to accept the decreased resolution in quantitative ability in order to measure expression levels of hundreds to thousands of genes simultaneously. Recent progress in micro PCR technology has enabled researchers to create a chip with a 32 x 32 array of 200 nl reaction volume chambers for high-throughput RT-qPCR. This new technology allows for 1024 simultaneous RT-qPCR reactions with as little as 5 starting copies of RNA in each well, effectively bridging the gap between the high-throughput capabilities of microarrays with the sensitivity of qPCR [14].

Because cell populations are heterogeneous, the gene expression varies significantly between cells. Population-based averaging cannot distinguish between the expression levels of different cells, but just measures an average expression of the population. Because of this, systems have been developed to measure gene expression at the single cell level. This enables research into the kinetics of gene expression; detecting changes in cell expression that population-based averaging would not measure (Figure 10).

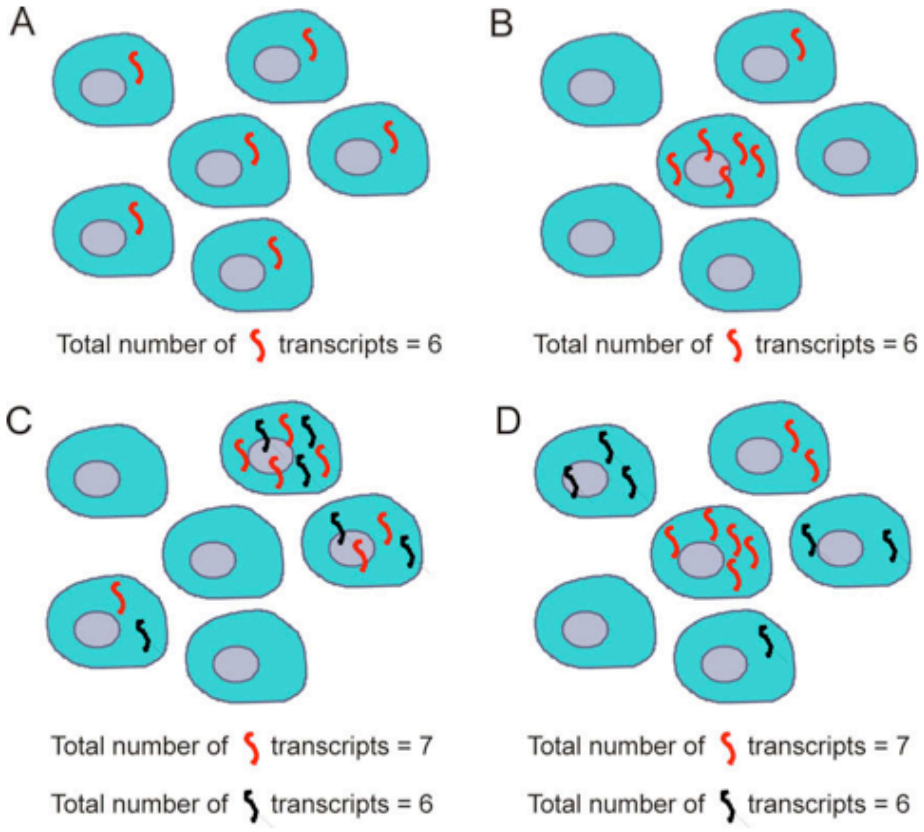

Figure 10: Gene expression levels of a cell population. Single-cell analysis enables researchers to distinguish between expression levels A) and B) as well as C) and D) while population based approaches do not [18].

In addition, researchers have worked to expand the spatial frequency of single-cell analysis, by separating and measuring the gene expression of 300 single-cells simultaneously [47].

A final area of micro-PCR research has been to develop systems with sample-in and answer-out capability. By minimizing the sample handling, researchers hope to both speed up the time by integrating all steps of the analysis into a single instrument, and to reduce sources of experimental error such as pipetting and evaporation by reducing the number of sample handling steps.

While significant advancements have been made in increasing the number of genes measured, achieving single-cell resolution, and integrating up-stream and down-stream processing steps, little work has been done in increasing the frequency of RT-qPCR measurements in the time domain.

CHAPTER 3

PROTOTYPE OPEN-LOOP SYSTEM

As previously shown, conventional techniques for gene expression measurement do not scale well in the time domain. The speed of reactions, large sample volumes, and expensive or non-reusable platforms add to the equipment and labor costs of such a test (Figure 7). In addition, current micro-PCR techniques do not scale well in the time domain. Micro-PCR devices either require lengthy set-up time, take hours to run, are complex and expensive to fabricate, are not easily disposable, or require sample handling between steps.

Ultimately, commercial implementation and the speed advantages of infrared PCR in microfluidic chips have been hindered by at least one of the following requirements for every amplification run: (1) thermocouple insertion time and complexity, (2) optical alignment with microscopic (i.e. sub mm) accuracy and repeatability, or (3) calibration. An inexpensive, easy to manufacture, disposable device with minimal set-up time, integrated upstream and downstream processing steps that takes advantage of the speed and small volumes offered by micro-PCR technology would allow researchers to measure gene expression in increments of hours rather than days.

We have designed, manufactured, and tested an infrared radiative thermocycler and associated microfluidic chip that retains the advantages of infrared PCR systems (e.g., speed, low volume, low power consumption, low cost, compact form) while eliminating the need for thermocouple insertion and repeated active alignment and calibration. Open-loop temperature control from a *single* calibration run is used for *multiple* consecutive amplifications on *multiple* identical instruments. This temperature control is made possible by passive, precision-engineered alignment fixtures, accurate and repeatable polymer microchip design and fabrication methods, and systematic thermal management strategies. We describe the instrument and chip design, fabrication,

and performance. We demonstrate its functionality with reproducible sub-10 min PCR amplification of a 500 bp amplicon from λ-phage.

Design overview

The system, shown in Figure 11, consists of a 1450 nm infrared laser diode with heat sink and fan, collimating lens with x-y stage, and microchip holder. As we have shown in previous work [52], this wavelength for infrared PCR is advantageous because it affords two orders of magnitude difference in absorption between the aqueous PCR solution and the surrounding polymer chip; an ideal environment for rapid cycling while retaining thermal isolation between adjacent chambers within a chip. The heat sink and fan keep the laser diode temperature and corresponding power output constant. The laser diode optical output power required is only 580 mW; the necessary electrical input power of 5 W is an order of magnitude less than all commercial thermocyclers and most research devices and thus facilitates portable and compact designs.

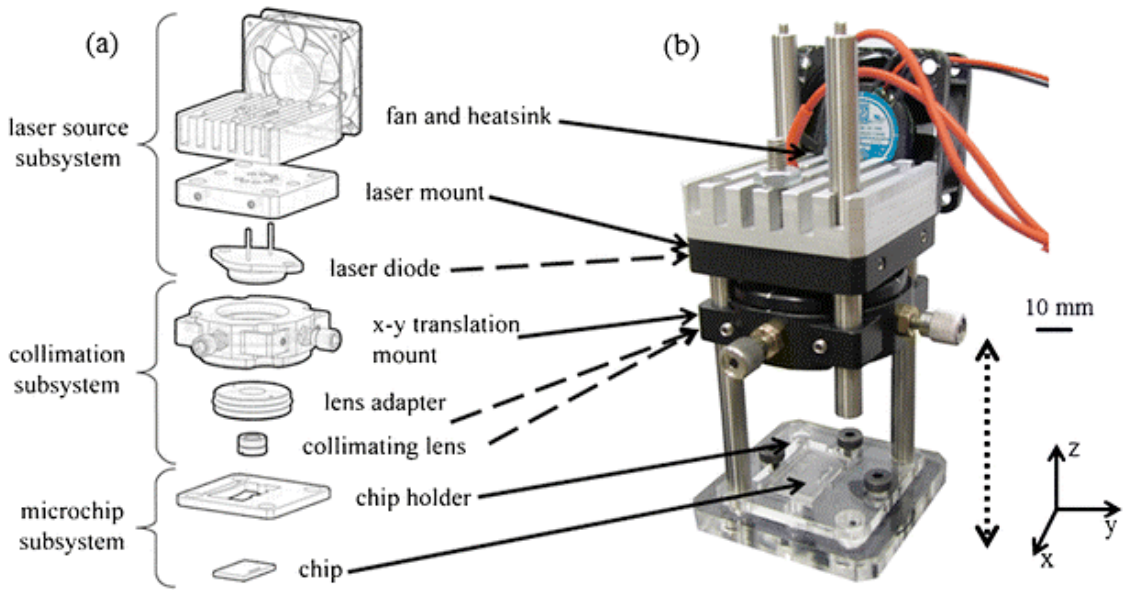

Figure 11: (a) Exploded view diagram of laser thermocycling system showing the laser source subsystem (*top*), collimation subsystem (*middle*), and microchip subsystem (*bottom*). *Dashed arrows* represent components that are embedded and not easily visible in the photograph. (b) Photograph of laser system, where the *dotted line arrow* represents the movement of the laser and lens assembly for loading the microchips into the chip holder.

The collimating lens and x-y stage are used to align the laser to a reaction chamber on the chip by burning a hole in a piece of toner paper (not shown) attached to the chip. The x-y stage is adjusted until the toner paper hole and microchip reaction chamber are directly aligned. The microfluidic chip holder is a single poly (methyl methacrylate) (PMMA) part, as seen in Figure 12(a), consisting of a leaf spring and three points for full kinematic constraint in the x-y plane. The entire assembly rests on a standard 30 mm cage system. Translation of the optical assembly on this rod system allows microfluidic chip insertion and removal. Associated electronics not shown in Figure 11 are the laser driver, power supply, and data acquisition board. These are sized similarly such that the total system volume is on the order of 200 mm^3.

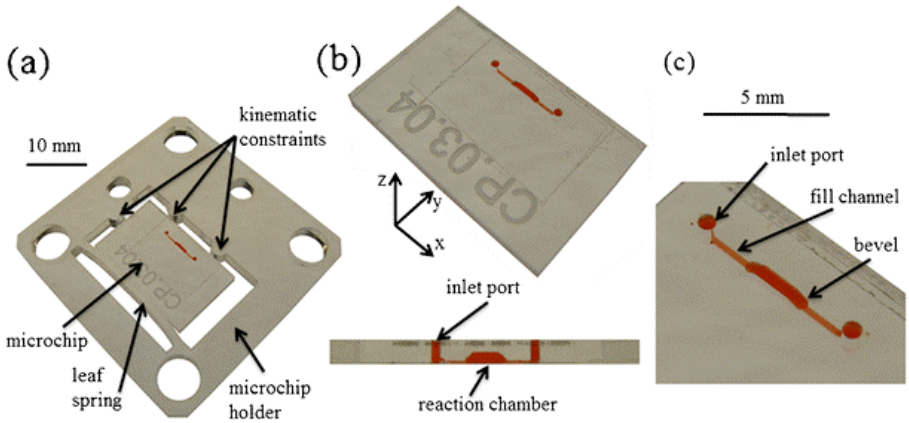

Figure 12: (a) Photograph of poly (methyl methacrylate) (PMMA) chip holder showing kinematic constraints, leaf spring, and microchip, (b) isometric view and side profile of PMMA microchip, (c) and close up of reaction chamber showing inlet port, fill channel, and beveled reaction chamber.

Using Labview, we implemented software for analog open-loop laser driving voltage control. The inputs (voltage, time) are run from a text file. To operate the system, the chip is filled with the requisite PCR solution, positioned, the laser assembly is lowered onto the chip, and the Labview program is initiated. The total amount of time for filling, sealing, and subsequently recovering the sample from the chips after the run with a pipettor is less than 1 min.

Polymer chip design and fabrication

The microchips, seen in Figure 12(b) and (c) feature inlet ports on both sides of the reaction chamber that allow standard pipette tips to easily fill the chamber. Narrow fill channels lead to the reaction chamber to minimize diffusion, and the beveled chamber geometry helps to ensure complete filling and easier thermocouple insertion when required for calibration. Microchips were fabricated from PMMA at a rate of two chips per minute, using a 3-axis vertical milling center (Haas, OM-1A) capable of accurate positioning within 10 μm and repeatability of 6 μm. The spindle operates at speeds up to 30,000 rpm, enabling the use of miniature end mills (Harvey Tool) and drill bits (Drill Bit City) with sub-millimeter diameters. These tools are zeroed to the polymer workpiece by

detecting electrical conductivity between the tool tip and the base of a custom aluminum fixture [53] that was milled and used to align and rigidly hold the polymer workpiece, since small part deflections can easily damage the fragile tooling. A corner relief was pocketed into the fixture along with features for interfacing with a standard vise to allow repeatable positioning. Strap clamps were laser cut from 3.175 mm acrylic, which was chosen to avoid marring the surface of the workpiece. These were configured in a third-class lever arrangement and the screws were hand-tightened to provide clamping force sufficient to overcome cutting forces. Toolpaths were manually written in G-code to achieve the relatively simple designs but can also be programmed using computer-aided manufacturing (CAM) software for complex geometries.

During the milling process, compressed air was used for clearing chips and preventing burr formation. Following milling, microchips were ethanol rinsed, dried with pure nitrogen, and the bottoms were sealed by a simple thermal bonding process with a 100 μm polymer film on a hot plate at 155°C, 30 min, and 100 psi for a 20 mm × 12 mm microchip. The top of the chip is sealed after filling with an optically transparent and biologically compatible adhesive film (Excel Scientific, ThermalSeal RT). Microchips have been used repeatedly without polymer delamination or damage, yet the adhesive film is easily peeled away manually.

This micro-milling process has been invaluable during the prototyping phase of this work. Altering a design and making a new batch of microchips can be easily accomplished in less than 1 day. Materials such as PMMA, polycarbonate, and a biocompatible grade of cyclic olefin copolymer (COC) have all been successfully used for a substrate. PMMA was chosen because it is most quickly machinable, while retaining excellent optical, thermal, and biocompatible properties [54]. Another advantage is the three-dimensional geometries attainable with micro-milling in order to create path lengths amenable to maximum absorption as well as control of the surface-

area-to-volume ratio for optimum heat transfer characteristics and minimal adsorption of biological reagents to the interior microchip surfaces.

Thermal modeling

To better understand how an aqueous solution within a polymer chamber is heated by radiation, a computational model (Matlab, Mathworks, Natick, MA) was created that predicts the radiation absorption as a function of distance through the aqueous solution, or pathlength. We have described in detail this approach earlier [52] and so summarize it here only briefly. First, the spectral irradiance of the source is scaled by integrating over its full spectrum and equating this with the measured total power output, yielding the spectral power distribution, $P_0(\lambda)$. This is then attenuated uniformly by accounting for losses due to reflection at the air-polymer interface. Finally, the power absorbed by the aqueous solution as a function of wavelength, $P_{ABS}(\lambda)$, is calculated using the Beer-Lambert Law as $P_{ABS}(\lambda) = P_0(\lambda)(1-10^{-\alpha(\lambda)l})$, where $\alpha(\lambda)$ is the wavelength dependent absorption coefficient of PMMA and l is the pathlength. Integration with respect to wavelength yields the total power absorbed as a function of distance. Applying this model to our microfluidic chip, aqueous solution, and laser resulted in 90% power absorption after 0.5 mm of radiation propagation through the solution (z-axis direction).

To compute the temperatures in the aqueous solution resulting from this radiation absorption, we implemented a finite element model (COMSOL, Stockholm, Sweden). We were most concerned with the temperature variation along the z-axis through the chamber in the direction of radiation propagation along the chamber centerline ($x = y = 0$), where the temperature is highest in the x-y plane. To implement the model, we divided the chamber into equal volumetric sections spanning the x-y cross-section, and assigned heat generation power to each of them based on the pathlength-dependent absorption model described above. For our design, we selected a total laser power output of 580 mW, absorbed by five volumetric sections in the direction of radiation propagation

absorption; each section 150 μm thick. Respectively, the radiation absorbed and corresponding centerline temperature of each section was 60.6% yielding 93.4°C, 21.1% yielding 90.2°C, 7.35% yielding 83.4°C, 2.56% yielding 77.7°C, and 0.89% yielding 73.1°C. Thus the total predicted temperature variation through the 750 μm deep chamber along the z-axis is 20.3°C. We experimentally measured a temperature gradient of 8°C with a thermocouple (T240-C, Physitemp, Clifton, NJ), and attribute the difference to the thermocouple's physical size of 130 μm in diameter and its location approximately 100 μm from the bottom of the chamber. These thermal modeling results proved useful in our calibration efforts.

Calibration

In order to utilize open-loop control, a calibration curve relating laser driving voltage to aqueous solution temperature is necessary. The calibration curve for our system is seen in Figure 13. The thermocouple used for calibration is heated directly by the laser, so calibration requires measuring and compensating for this bias error as follows. First, it was known that the threshold voltage for the laser to turn on was 0.25 V. At this driving voltage the bias is zero and the thermocouple reads a temperature of 33°C, identical to the chamber temperature. Next, the driving voltage was increased as the reaction chamber was observed with a microscope. Boiling, as indicated by the rapid formation and expansion of bubbles in the chamber, occurred at 1.1 V and corresponds to 100°C at atmospheric pressure.

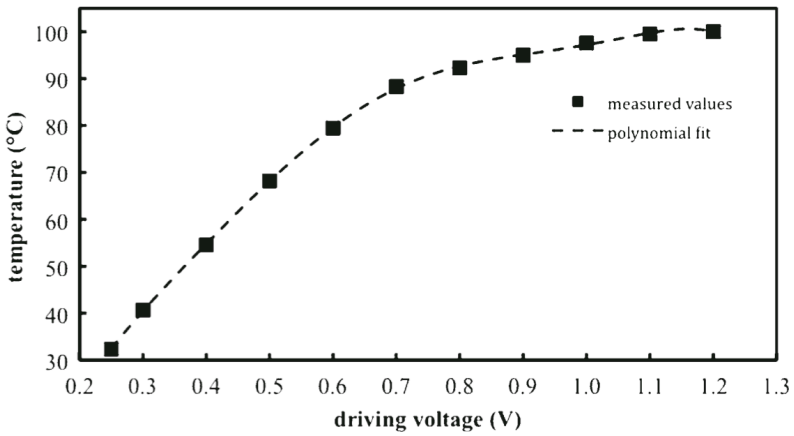

Figure 13: Calibration curve relating laser driving voltage and aqueous solution steady state temperature used for open-loop temperature control.

With the thermocouple centered and positioned at the bottom of the chamber, the measured bias increases from 0°C at 0.25 V to around 8°C at 1.1 V. The variables affecting this bias include thermocouple placement repeatability, bubble formation, and direction the thermocouple tip is bent. A special calibration microchip was manufactured with the thermocouple bonded to the bottom layer. This prevents many of these variations between runs because the thermocouple tip is in the same position every time. Also, since our thermal modeling predicted that 90% of the radiation is absorbed in the first 0.5 mm of the aqueous solution, confounding effects of radiation heating of the thermocouple directly were minimized with the thermocouple located at the bottom of the chamber. A polynomial was fit to the bias corrected temperature measurements, resulting in the calibration curve shown in Figure 13.

Once this curve is created, it can be used to find the three voltages corresponding to the denaturing, annealing, and extension temperatures of the particular amplification to be performed. While these three voltages are all that is required, slow temperature ramping under such a simple control scheme would necessitate hours for one amplification run. Therefore, to expedite heating and cooling, we applied the maximum driving voltage and then a holding voltage corresponding to the denaturing temperature.

Similarly for cooling, a zero voltage duration precedes the annealing voltage. A typical three temperature PCR cycling program thus requires five distinct driving voltages: maximum power to ramp up to denaturing, a denaturing holding voltage, zero voltage to cool to annealing, an annealing holding voltage, and an extension holding voltage. If there is a significant temperature difference between the annealing and extension temperatures, a sixth full power ramping voltage can be implemented between those two holds. The heating and cooling times are measured and set to minimize under- and over-shoot. The resulting temperature profile and driving voltage can be seen in Figure 14. Desired times and temperatures were 4 s at 90°C for denaturing, 5 s at 68°C for annealing, and 5 s at 72°C for extension.

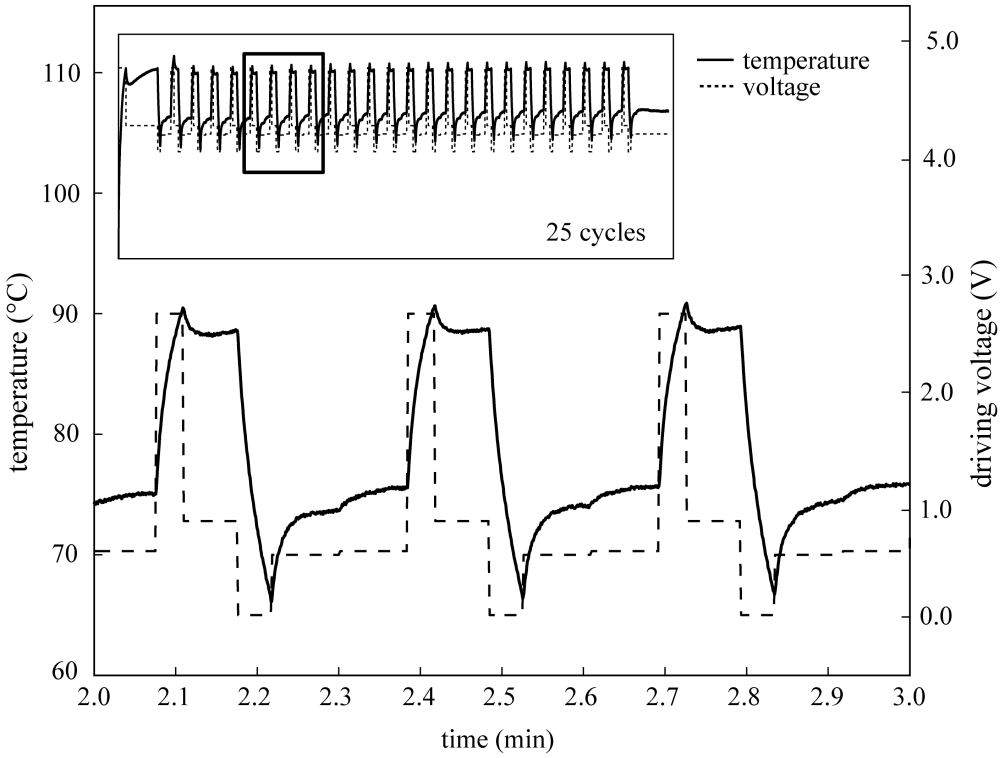

Figure 14: Experimental temperatures obtained from calibration and corresponding laser open-loop control voltages for PCR of 500 bp DNA amplicon in 9:58 in a 1 μL chamber within a polymer microfluidic chip.

Mechanical and thermal repeatability

In order for open-loop control to work consistently, thermal and mechanical repeatability are paramount. As described previously, the x-y stage to position the collimating lens is only adjusted once. However, the laser beam alignment is periodically checked to ensure identical heating by burning a piece of toner paper as mentioned previously. Although it is rarely out of alignment, this test takes less than 1 min to perform and ensures consistency.

To measure the repeatability of the chip alignment in the holder, we mounted the system on an inverted microscope (Nikon, TE2000-E) to image the chip location during repeated placement. Of the three principal system axes, shown in Figure 11, the x-axis error is insensitive because this axis is parallel to the reaction chamber's length and deviations less than 1 mm do not cause significant temperature differences. For the y-axis alignment repeatability measurement, we placed and imaged the chip five times. The standard deviation measured was $\sigma_y = 5.31$ μm, causing no measurable temperature difference with thermocouple inserted into the chamber and laser heating. This same test is repeated each time a new batch of chips is made to make sure they are within specification.

For the z-axis repeatability measurement, or direction normal to the chip surface, we repeatedly focused the microscope on either a stationary chip or a successively removed and replaced chip. From the stationary chip, we ascertained from five measurements that the standard deviation of the focusing error was 9.9 μm. From five measurements with the replaced chip, which includes this focusing error, the standard deviation of the position measured was $\sigma_z = 16.4$ μm. To determine if this error was problematic, we measured the temperature variation corresponding to z-axis translation between the laser and chip. For a 1,000 μm displacement, more than the 750 μm chamber height, a temperature variation of only 0.5°C was measured, so the σ_z measured was deemed acceptable.

To measure the *combined* repeatability of the chip placement, laser z-axis translation to allow chip placement, laser power output, and thermocouple placement for calibration, we successively removed, replaced, and heated a water-filled chip and its thermocouple. Five consecutive temperature measurements showed a standard deviation of 0.1°C, well within tolerances for PCR from conventional instruments. We note that the primary cause of the difference in temperatures between the trials is the result of variations in thermocouple placement, which is not used during PCR.

PCR amplification of λ-phage DNA

As a means to verify our system and method, an amplification of λ-phage DNA was performed on both our laser-based system and a conventional Peltier-based thermocycler (BioRad, MJ Mini). The reaction solution was prepared in quantities of 5 μL volumes according to the following protocol: 0.5 μL10X PCR buffer, 0.8 μL $MgCL_2$ (25 mM), 0.1 μL dNTP mixture (10 mM), 0.1 μL forward and reverse primers (20 μM), 1.2 μL BSA (1 mg/mL), 1.0 μL DNA (45.8 μg/mL), 1.2 μL water, and 0.1 μL Taq polymerase. BSA has previously been shown to aid microchip PCR [20]. The primer sequences used were 5′-GATGAGTTCGTGTTCGTACAACTGG-3′ for the forward primer and 5′-GGTTATCGAAATCAGCCACAGCGCC-3′ for the reverse primer. Our microchips were loaded with about 1,400 nL, of which approximately 820 nL was located within the chamber. After running the 25-cycle program as seen in Figure 14, we evaluated results with microchannel electrophoresis separation (Agilent, Bioanalyzer). Successful amplification with excellent signal to noise ratio (>200:1), for a typical trial are shown in Fig. 5.

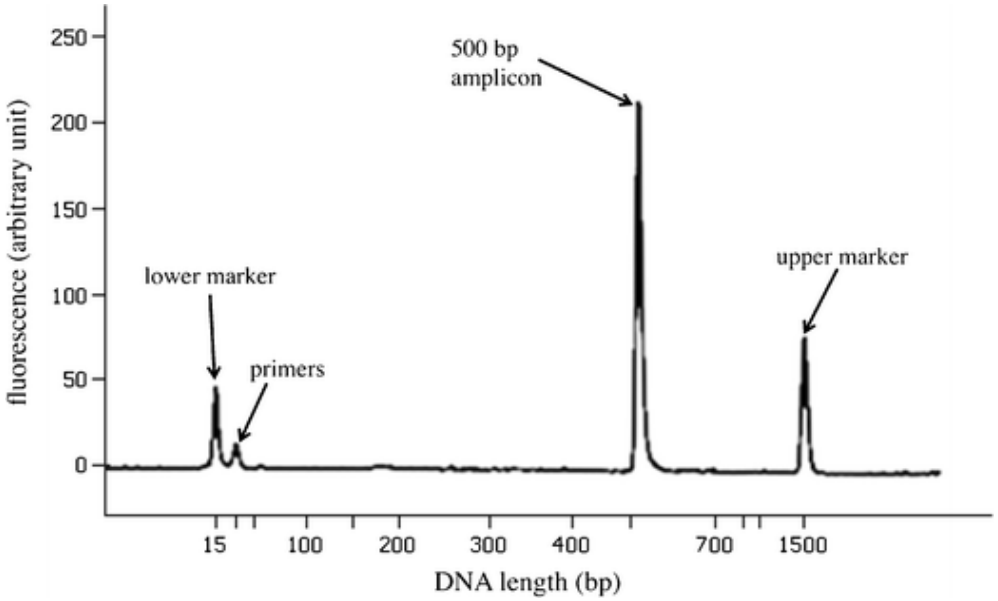

Figure 15: Electropherogram of 500 base pair lambda DNA amplification performed in less than 10 min on a 1 μL polymer microchip. This was repeated five times with identical results.

This amplification was performed in less than 10 min, with a total setup, recovery, and run time of less than 12 min. Five identical runs were performed in series with the same outcome, demonstrating the repeatable DNA amplification achievable with our device.

It should be noted that the calibration curve is unique to the microfluidic chip design and laser used. However, these variables are easy to maintain, and we have used the same calibration curve on two identical laser thermocycler systems that we have constructed to obtain DNA amplification with no adjustments. If a new microchip design or a different laser is used, the calibration curve can be created in approximately 3 h. This process has an initial time investment, but greatly reduces the amount of time needed for each machine run.

Conclusions

The operation of this plug-and-play infrared-mediated PCR system has the advantages previously seen in microfluidic PCR systems, but operates more like a

conventional PCR instrument in that the user simply loads and places the chip or well plate into the instrument, and removes it following amplification for sample post-processing. From a precision optical and mechanical design, thermal modeling, control, and calibration we were able to show repeatable DNA amplification in less than 10 min on a microchip of a volume of less than 1 μL in a system that requires little user interface and has a total run time of less than 12 min. This approach is not restricted to low-cost microfluidic volumes (e.g., 1 μL), thus increasing utility. We have previously cycled 10 μL with our prototype using standard PCR tubes in place of the microchip. With higher laser power and beam size control, we can cycle these larger volumes faster than conventional instruments while maintaining the advantages of open-loop and potentially multiplexed temperature control. Also, scaling up to multiple reaction chambers on one microchip can now be achieved without having to simultaneously scale up the temperature measurement system. If the radiation is optically manipulated, there is potential for unprecedented scalability and independent temperature control of multiple PCR chambers on a single microchip. The open-loop control scheme allows this to be done in a similar total time as the one reaction chamber chip.

Analysis of Prototype Open-Loop System

By utilizing infrared heating with open-loop control, as well as repeatable chip manufacturing and alignment techniques, our open-loop PCR system was able to achieve rapid amplification of DNA with minimal set-up time. However, the amplification efficiency of the system was still significantly less than traditional bench top thermocyclers (Figure 16).

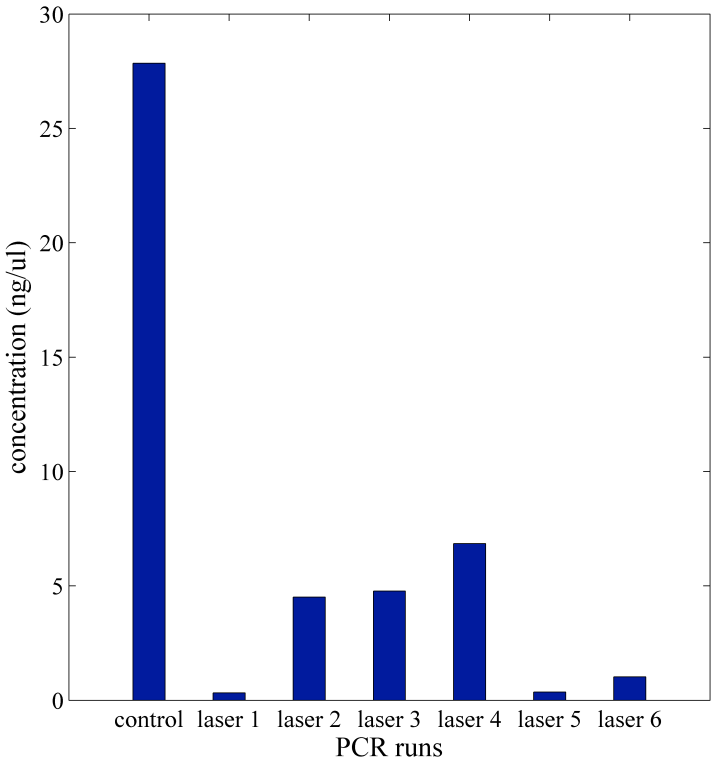

Figure 16: Final concentrations of PCR product from amplifications performed in a conventional thermocycler, labeled as control, and performed with the open-loop laser system, labeled as laser 1 - 6. The final concentrations of PCR product from the laser system were statistically different than the thermocycler control, indicating the laser system is not as efficient as current techniques.

To test if the final concentration of PCR products from the two systems was statistically different, a two-sample t-test was used. A null hypothesis that the two means were equal was assumed and evaluated at a 1% significance level. The test produced an h = 1 and p = 4.0952e-4, which rejected the null hypothesis that the two means were equal. This test indicated that the final PCR product concentrations from the prototype open-loop system were statistically less than conventional thermocyclers.

CHAPTER 4

THERMAL IMPROVEMENTS

PCR is a temperature-controlled and enzyme-catalyzed biochemical reaction that requires temperature accuracy and stability for efficient DNA amplifications. Non-optimal temperatures can result in only partial denaturation of the DNA, inhibition of Taq polymerase, formation of primer-dimers, or only partial extension of the DNA sequence being amplified, which contribute to both reduced PCR yield and the formation of non-specific PCR products [20]. The prototype open-loop PCR system previously discussed represented a milestone for micro PCR systems in terms of speed and ease-of-use. However the temperature accuracy and stability was not comparable to conventional machines. The standard deviation of temperatures for the denaturing, annealing, and extension cycles were σ_d = 1.3 °C, σ_a = 2.0 °C, and σ_e = 0.75 °C respectively and the average cycle-to-cycle variation for denaturation, annealing, and extension temperatures was σ_d = 0.87 °C, σ_a = 0.39 °C, and σ_e = 0.74 °C respectively. In addition, a run-to-run temperature variation of up to 8 °C was noted. The multiple sources of error that contributed to these effects were divided into five areas to be addressed: temperature dynamics of one cycle, temperature dynamics across multiple cycles, variation between runs, random fluctuations in measured temperature, and variations in laser power output.

Temperature Undershoot and Overshoot

The non-optimal temperature dynamics of one PCR cycle was a result of the temperature undershoot and overshoot from the desired hold temperature when transitioning from one steady-state temperature hold to another (Figure 17).

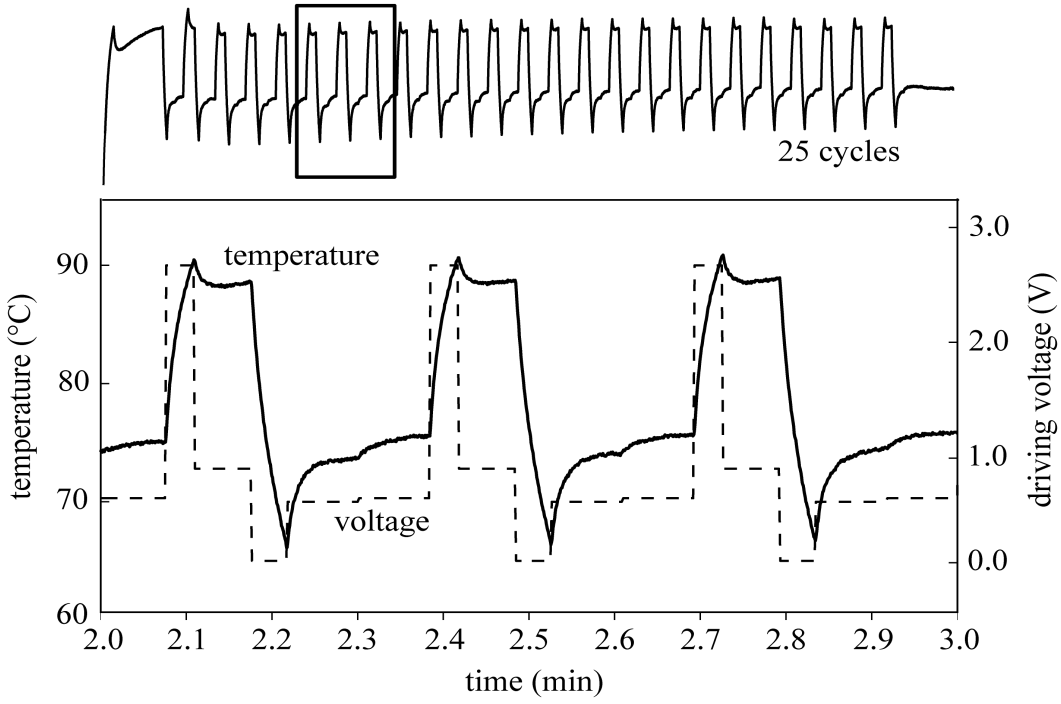

Figure 17: Experimentally measured temperatures and corresponding laser drive voltages for 3 PCR cycles. Inputting laser power in the form of square waves resulted in temperature undershoot and overshoot from desired hold temperatures.

Although the PCR solution was being directly heated by the infrared laser, the PMMA chip containing the reaction was also heating and cooling during the transitions from one temperature hold to another, causing the relationship between laser power and chamber temperature to shift. Therefore, assuming the system was always in steady state and inputting a square-wave steady-state power profile was not an accurate assumption and instead caused the temperatures to undershoot and overshoot for each cycle (Figure 17).

Optimized Laser Power Profiles

The solution to this problem was to input dynamic, exponentially increasing and decreasing power profiles to minimize the temperature undershoot and overshoot of the system. These power profiles were determined empirically based upon the heating and cooling rates of the reaction chip. To accomplish this, a calibration chip with a thermocouple was placed in the system. The system was cycled through the denaturing, annealing, and extension temperatures, with two minute holds at each temperature to ensure the system had reached steady state. The data was then analyzed to determine the approximate heating and cooling rates of the system when transitioning from one temperature hold to another by measuring the time it took for the chamber temperature to reach the steady state value. Using this information, dynamic, exponentially increasing and decreasing power profiles were created in MATLAB of the form,

$$\text{voltage} = a \times \log(b \times t) + c \qquad \text{(Eq. 2)}$$

where a, b, and c are constants determined empirically from the heating and cooling rates of the system and t is the hold time vector. The resultant power profile was a piecewise continuous function consisting of the exponential powers for each of the three hold temperatures between segments of maximum power and no power to achieve maximum heating and cooling rates.

Once an optimized power profile was created, it was tested and the temperature stability for the denaturation, annealing, and extension profiles was measured. Based on the system response, the profile was adjusted and the process repeated as necessary to obtain steady temperature holds. While this process required several hours, once created, a power profile does not need further adjusting. These optimal laser power profiles

greatly improved the steady-state temperature holds and decreased the standard deviation of denaturing, annealing, and extension temperature to $\sigma_d = 0.16$ °C, $\sigma_a = 0.18$ °C, and $\sigma_e = 0.15$ °C respectively (Figure 18).

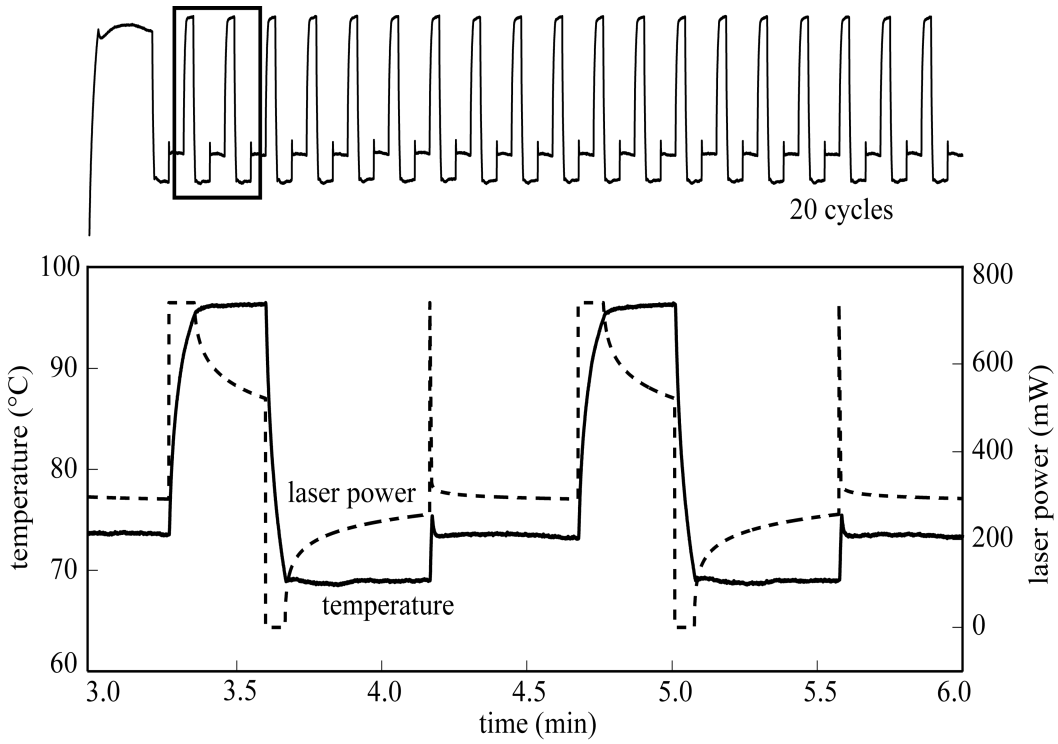

Figure 18: Experimentally measured temperatures and corresponding laser voltage profiles for two PCR cycles. Inputting exponentially increasing and decreasing laser power profiles resulted in steady temperature holds, minimizing temperature undershoot and overshoot.

Temperature Dynamics Across Multiple Cycles

During a 20 or 30 cycle PCR program, the average temperature for each of the denaturing, annealing, and extension steps was found to be increasing by up to 3 °C. While these fluctuations varied from run to run, the values generally increased during the first 5-10 cycles of PCR, before then settling upon steady-state values (Figure 19).

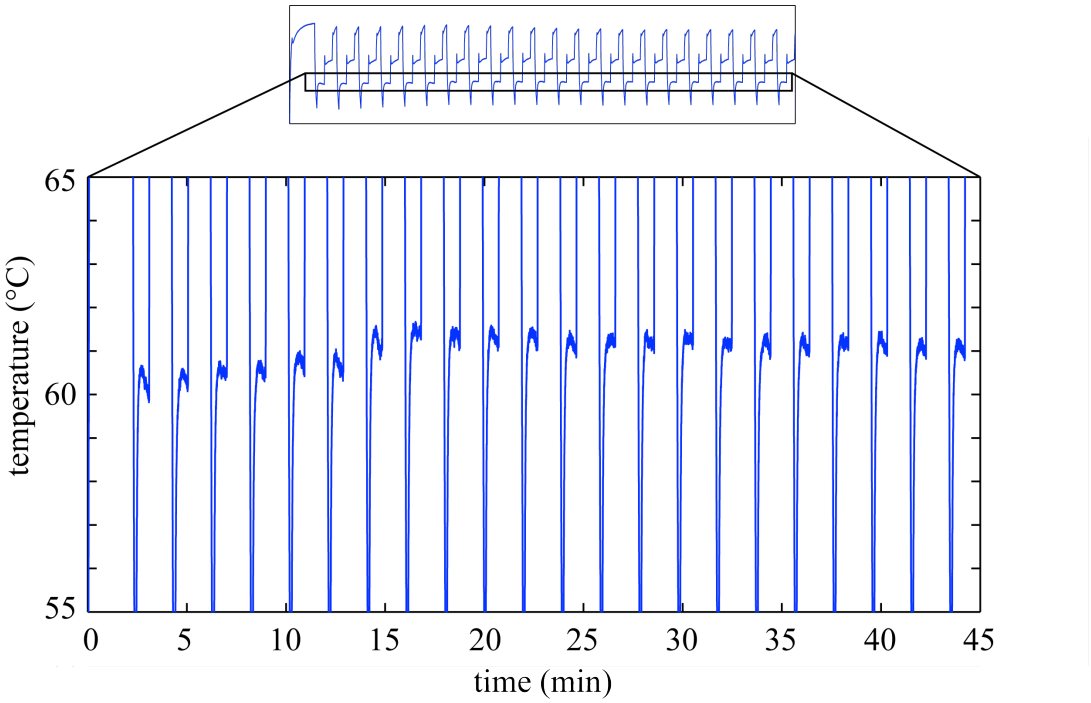

Figure 19: Experimentally measured temperatures for 22 PCR cycles. As the program progressed, the temperature holds for a given laser power input gradually increased over the first 8 cycles before reaching steady state conditions.

This indicated that not only was the area around the chamber heating and cooling, causing undershoot and overshoot from the desired steady-state temperatures, but that the entire chip was also gradually heating up during the first 5-10 cycles, before reaching a dynamic steady-state with the environment.

To test this theory, a calibration chip was preheated to different temperatures, filled with PCR solution, and run on the device. It was found that the starting temperature of the acrylic chip had a major impact on the steady-state temperature of the chamber over the first 5-10 cycles, before the chip settled into a state of equilibrium, likely causing the gradual temperature increase (Figure 20).

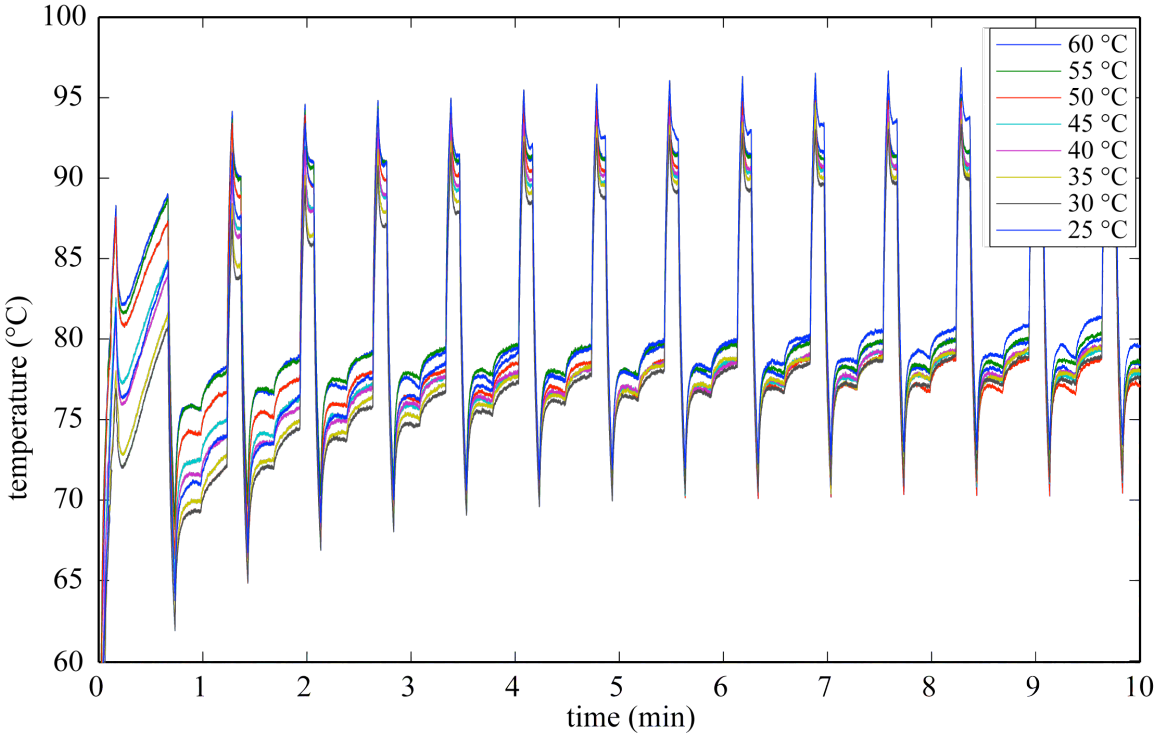

Figure 20: Experimentally measured chamber temperature as a function of time for different starting temperatures of PMMA calibration chip. A PMMA chip was preheated on a hotplate to various temperatures and run on the device.

Variation between runs

In addition to the temperature dynamics varying across multiple cycles, it was found that the steady state temperature of the chamber varied between runs as well. While this was partly due to chip misalignment, the variation also occurred when the same calibration chip was run on the device multiple times (Figure 21).

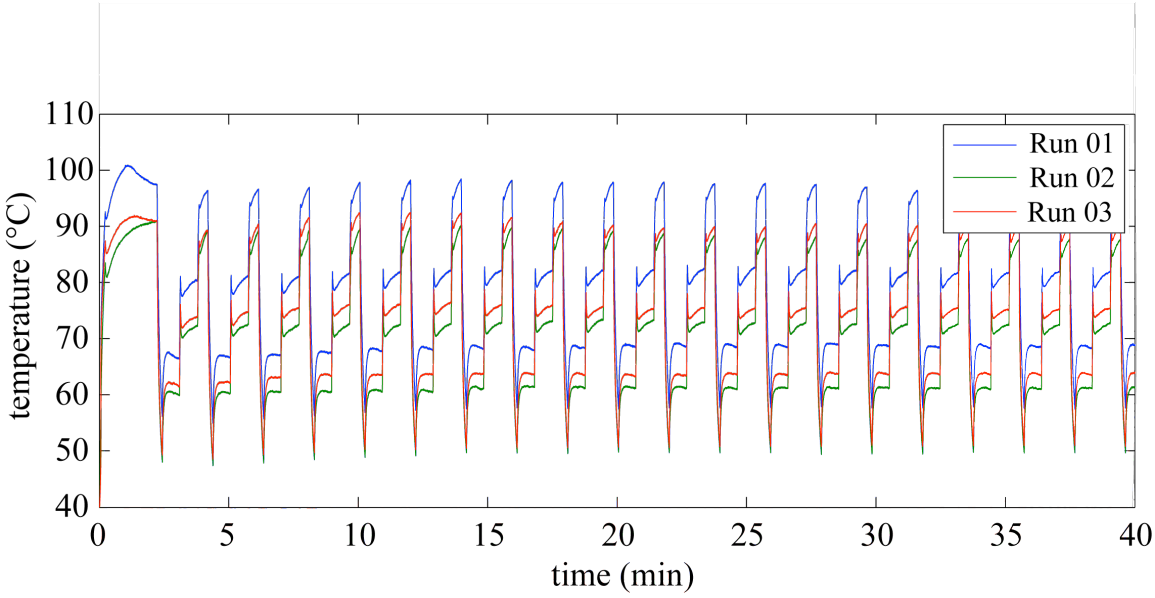

Figure 21: Experimentally measured chamber temperatures for 3 PCR runs. The same open-loop program was run on the same calibration chip. Variations in environmental conditions created variations in steady state temperatures.

The resulting variation in steady-state temperatures was likely a result of the environment around the chip changing temperatures between runs. The increase in environmental temperature was caused by conditions in the lab at the time of the experiment and by localized heating of the air around the chip due to heat dissipation by a CCD camera, microscope, computer, laser driver, laser diode, data acquisition system, and a halogen light source.

ANSYS Simulation

An ANSYS simulated was created to quantify the effect of environmental temperature on steady-state chamber temperature for a given power input. This simulation, created with ANSYS workbench, used a 3D transient thermal solver. The system geometry was created in Solid Works and imported into the ANSYS workbench. An internal heat generation region was selected as the reaction chamber, and the power profile imported into the model. The solid bodies were modeled with SOLID87 elements, surfaces modeled with TARGE170 elements, and contact regions modeled with

CONTA174 elements. The mesh was auto-generated using ANSYS Workbench with a minimum edge length of 1.7067 e-5 meters and an average contact surface length of 0.10204 e-2 meters. A contact tolerance value of 4.8881 e-4 meters was chosen between surfaces. A time step of 0.1 seconds was chosen and the model was run for 5000 seconds. Material properties for acrylic, water, and air were selected for the reaction chip, PCR solution, and environment respectively. The model was then validated by running a program with a known response and the predicted response from the model was compared to the measured chamber temperature (Figure 22).

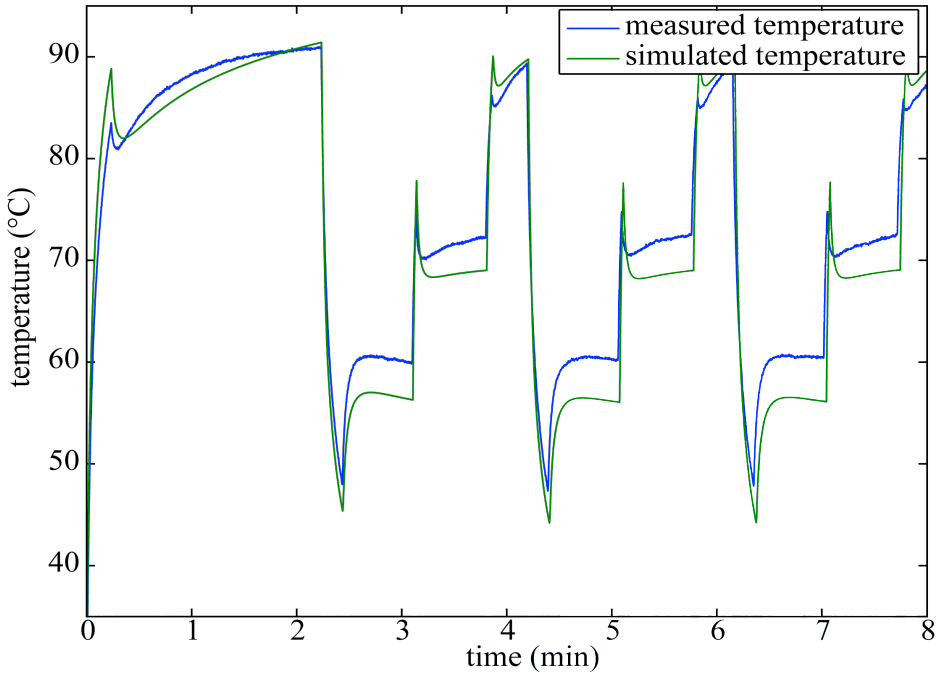

Figure 22: Experimentally measured temperatures and predicted temperatures from an ANSYS transient thermal model of the system.

After validation, the ANSYS simulation was used to quantify the effect of environmental conditions on the chamber temperature. The simulation of the setup was run once with ambient conditions at 25 °C, and once at 30 °C. It was found that a 5 °C change in environmental temperature resulted in an 8 °C change in chamber temperature, indicating that the environment around the setup strongly influenced the steady state temperature of the chamber (Figure 23).

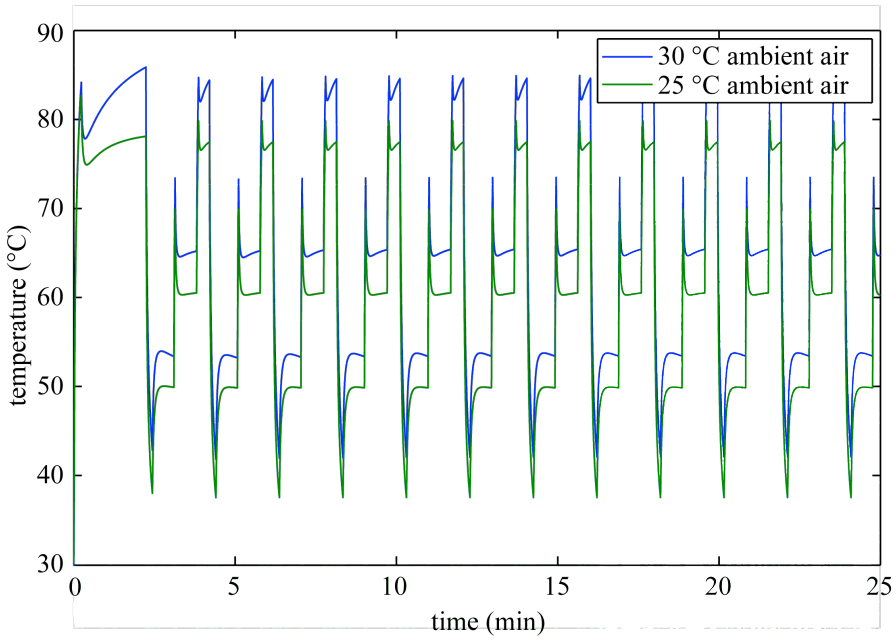

Figure 23: ANSYS simulations of chamber temperature for the same input laser powers given environmental temperatures of 25 °C and 30 °C.

Environmental Control

The results of the experiments indicated that the temperature of the chip as well as the environmental conditions around the chip strongly influenced the chamber temperature. Unless the environment could be accurately assumed to be a heat sink with a constant temperature, complicated environmental conditions including accounting for changing chip temperatures, environmental temperatures, and ambient temperatures would have to be included in the determination of the optimal laser power profile, significantly increasing the complexity of the procedure, and decreasing the robustness of the resulting PCR device (Figure 24).

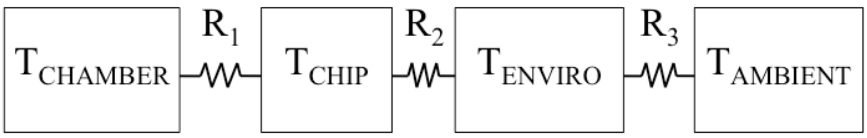

Figure 24: 1-D heat conduction model of system. Chamber temperature depends upon chip temperature, local environmental temperature, and ambient temperature.

The solution to both these source of error was to keep the temperature of the environment around the chip constant. Therefore, water cooled copper heat sinks were added to the system. Sandwiching the PMMA chip between these plates ensured that the environment around the chip would remain constant across multiple cycles, and through multiple PCR runs, regardless of room temperature or the temperature of the chip when loaded into the system. The implementation of the environmental chamber ensured that the environment around the chip could be assumed to be a constant temperature heat sink and only changing chip temperatures would have to be accounted for (Figure 25).

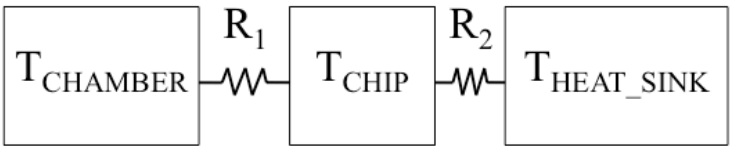

Figure 25: 1-D heat conduction model of system with environmental control. Chamber temperature depends upon chip temperature and heat sink temperature, which is a constant and simplifies the model.

This environmental chamber decreased the standard deviation of average temperatures across multiple cycles from $\sigma = 0.54$ °C to $\sigma = 0.08$ °C and the standard deviation of temperatures across multiple runs decreased from $\sigma = 4.5$ °C to $\sigma = 0.12$ °C (Figure 26).

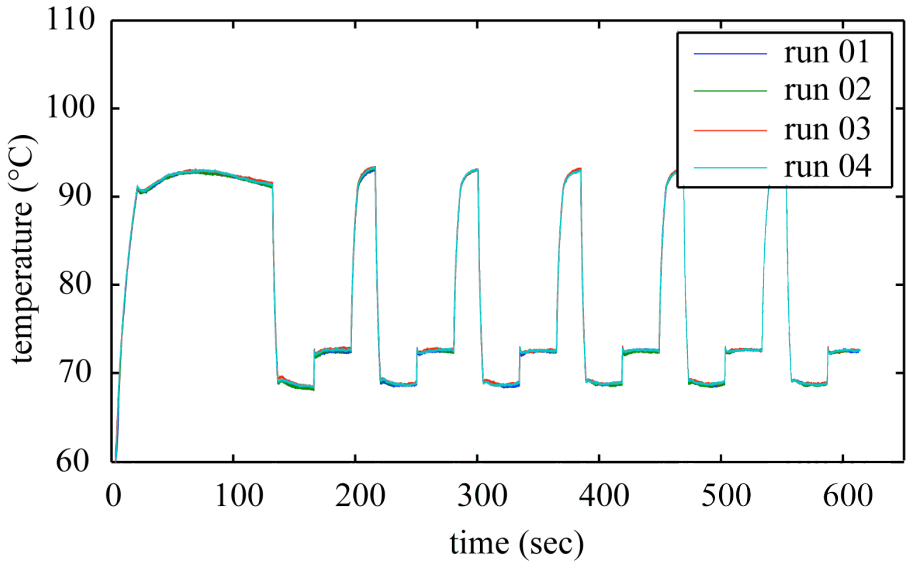

Figure 26: Experimentally measured temperatures for four PCR runs. Creating constant environmental conditions around the chip allowed for repeatable temperatures.

Random fluctuations and perturbations in measured temperature

Bubble formation in device channels is a serious problem for microfluidic experiments. This problem is especially critical for micro PCR devices that are subject to repeated temperature changes. Researchers have hypothesized that bubble generation occurs due to either the result of flow-induced trapping of air in micro cavities during the sample loading process or due to the expansion of micro air pockets within a bonded interface upon heating [55]. Despite knowledge about how they form, it is impossible to completely eliminate the entrainment of air when thermally bonding or filling a microfluidic device such as the PMMA chips we employ in our open-loop devices. However the problem can not be ignored as bubble formation in these chips often leads to random fluctuations and perturbations in the measured chamber temperature, especially when heated above 85 °C (Figure 27).

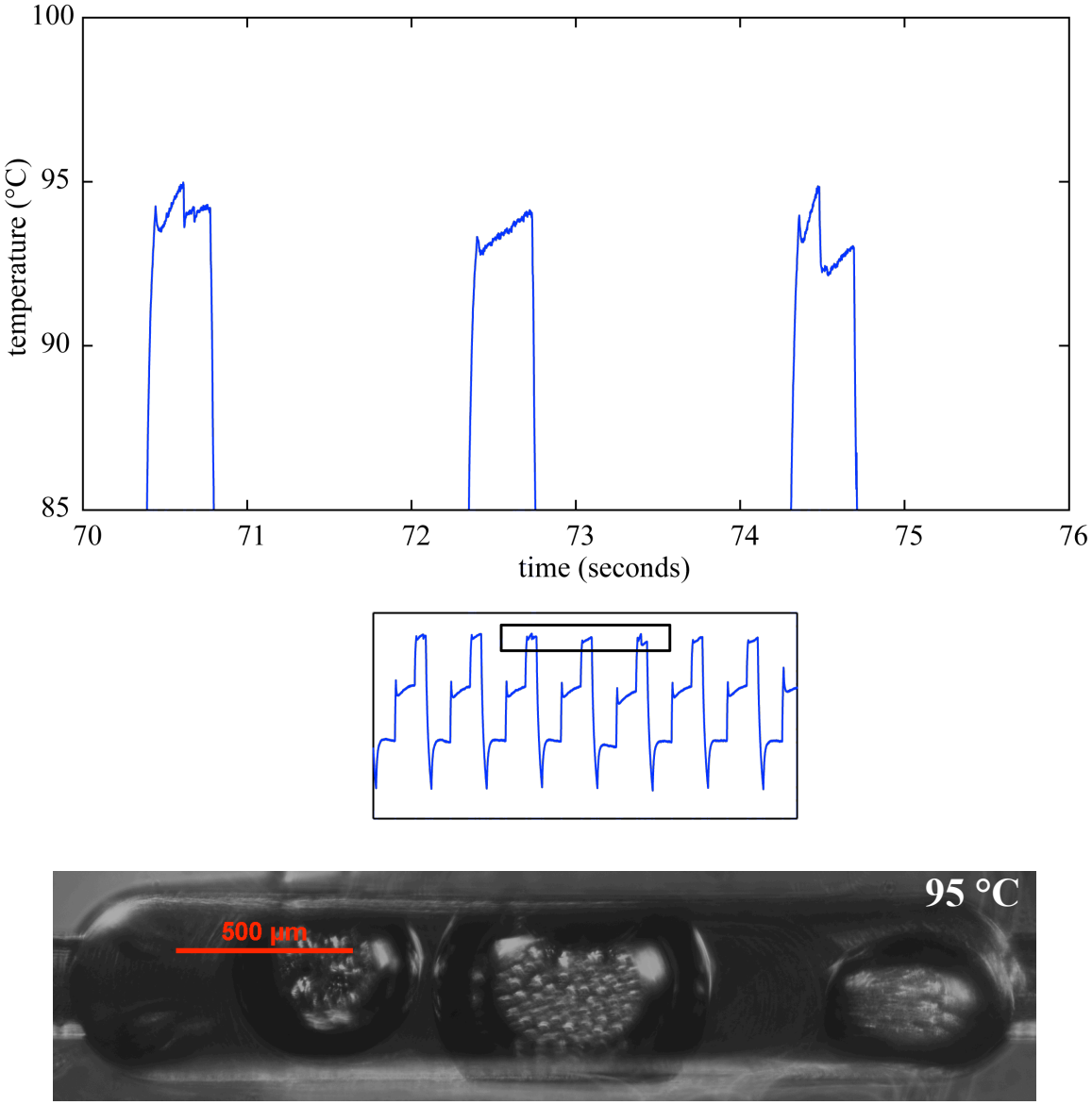

Figure 27: Bubble expansion in reaction chamber at higher temperatures causes fluctuations in temperature measurements as well as depletion of the sample during PCR runs.

These bubbles not only interfere with temperature measurements but also deplete the sample during a PCR run, causing dilution of or even the complete depletion of PCR product (Figure 27). One common solution among micro PCR devices is to lower the denaturation temperature to 91 °C to lessen the amount of bubbles that form. However lower denaturation temperatures can lead to only partial denaturation of the DNA strand, increasing the variability in PCR results [20].

Chamber Pressurization

Bubble formation depends upon the resultant magnitude of three forces: the outer surroundings force, surface tension force, and gas expansion force (Figure 28). Bubble expansion occurs when the gas expansion force is greater than the surface tension force and outer surroundings force and bubble suppression occurs when the force of the outer surroundings combined with the surface tension force is greater than the gas expansion force. For a reaction with a constant surface tension, the only option is to increase the force of the outer surroundings.

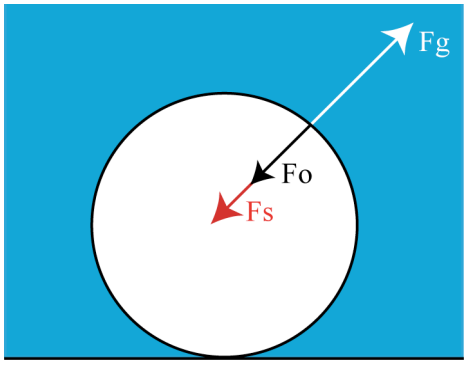

Figure 28: Diagram of bubble showing gas expansion force (Fg), outer surroundings force (Fo), and surface tension force (Fs).

To accomplish this, the reaction chamber was pressurized with compressed nitrogen to 40 psig. A pressure manifold was constructed so that the two fill ports of the

chip were equally pressurized when loaded into the device preventing the sample from shifting in the chamber upon pressurization. This resulted in the elimination of bubbles in the channel over the range of temperatures necessary for PCR (Figure 29).

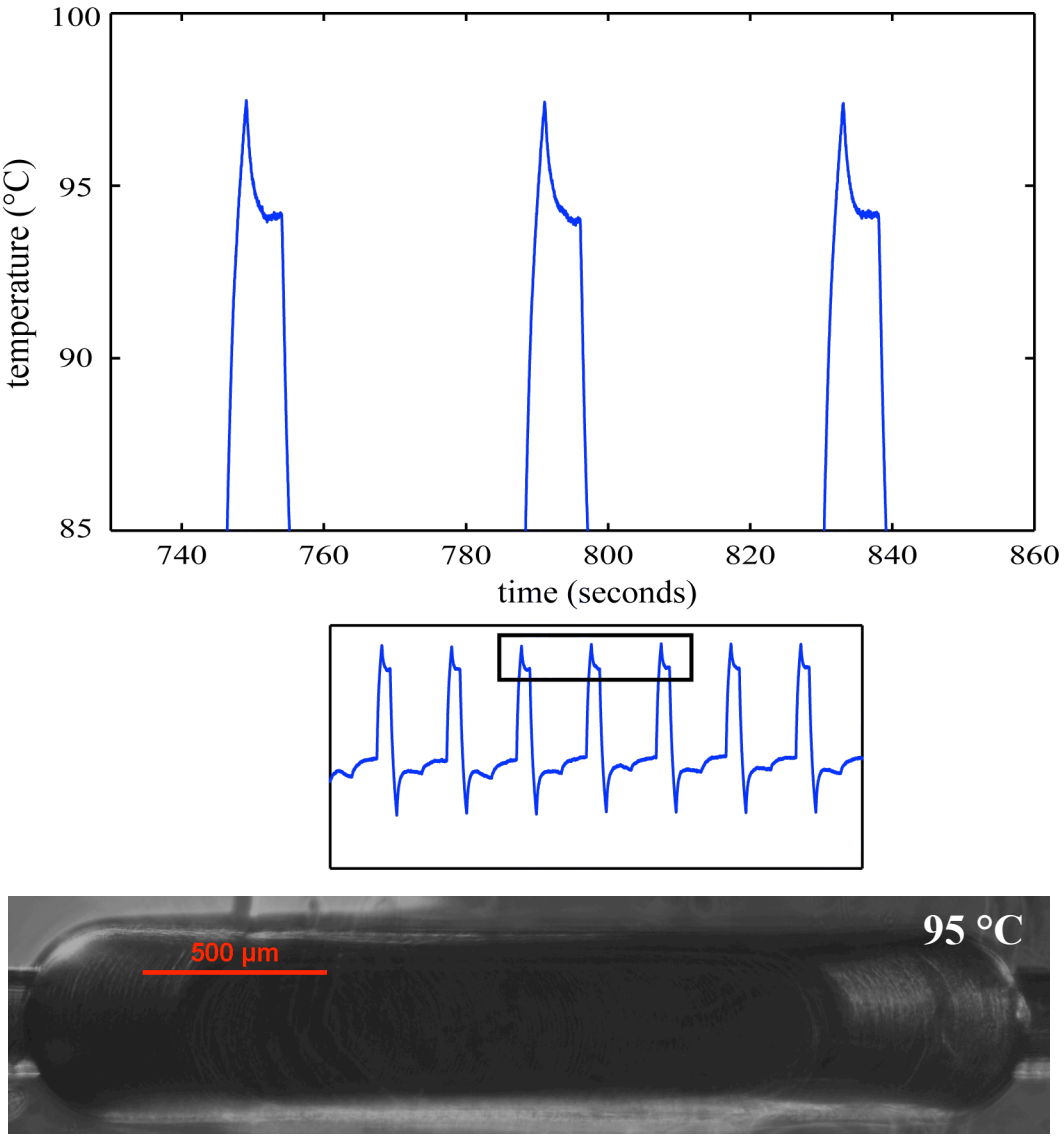

Figure 29: Pressurization of the chamber prevented bubble nucleation and expansion upon heating resulting in uniform temperature measurements and no sample depletion at high temperatures.

Overheating of Laser Diode

The device uses a 1450 nm infrared laser diode to heat the PCR solution. While they are inexpensive and have relatively low power consumption, their performance is highly temperature dependent. Therefore, adequate cooling of the diode is important for stable power outputs. To accomplish this, a copper heat sink was added to the top of the laser subassembly, and the same constant temperature water was flowed through this assembly as the environmental chamber. The addition of this a heat sink greatly increased the stability of power output from a standard deviation of $\sigma = 17$ mW at 560 mW to a standard deviation of $\sigma = 5.0$ mW at 560 mW (Figure 30).

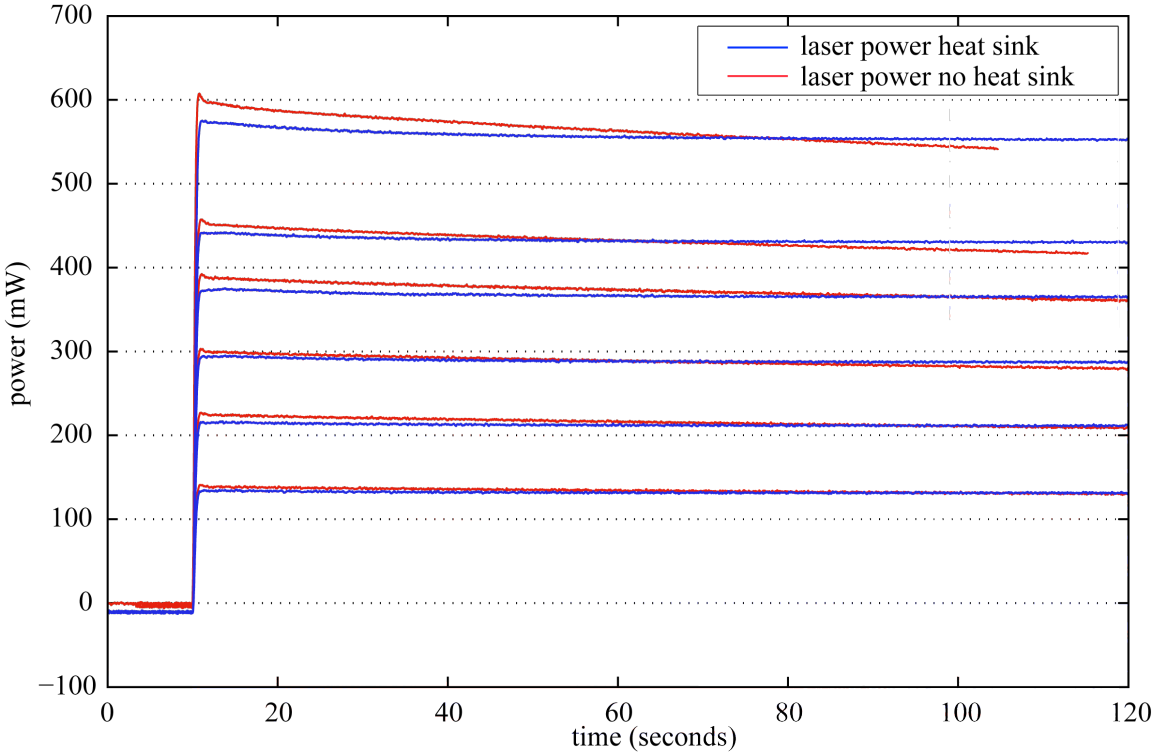

Figure 30: Laser diode power output is highly temperature dependent. With no heat sink, power output decays rapidly above 200 mW but with the addition of a water cooled copper heat sink remains stable up to 560 mW.

CHAPTER 5

CHIP MANUFACTURING AND ALIGNMENT IMPROVEMENTS

The success of a micro PCR device with open-loop control is not limited to ensuring the thermal stability of the system. It is also dependent upon repeatable manufacturing and positioning of *identical* PMMA reaction chips. Slight differences in the alignment of the chip or differences in the chamber reaction volume were found to inhibit the system's ability to perform repeatable, efficient PCR amplifications.

Chip Machining

As previously discussed, the microchips for PCR were fabricated from PMMA using a 3-axis vertical milling center (Haas, OM-1A) capable of accurate positioning within 10 μm and repeatability of 6 μm. A machining fixture with a 3 x 4 array of slots for chips was created so that up to 12 chips could be machined at once. The 12 mm x 20 mm PMMA chip blanks were laser cut from sheets of 1.50 mm cast PMMA (McMaster-Carr). While nominally 1.50 mm thick, the casting process creates ripples in the sheet, causing variations in thickness across the entire sheet. These variations were quantified and for a batch of 96 PMMA chips, the thicknesses ranged anywhere from 1.66 mm to 1.79 mm thick (Figure 31).

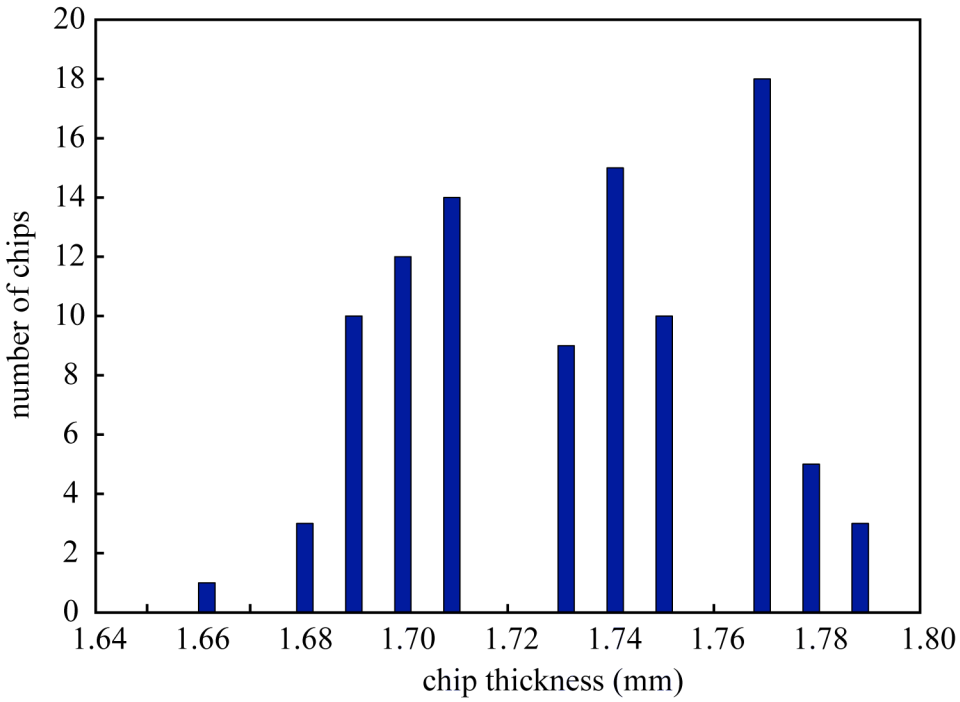

Figure 31: Histogram of a batch of 100 laser cut PMMA chips from a sheet of 1.50 mm cast PMMA. Variations in sheet thickness are a normal part of the casting process and must be accounted for when fabricating PCR reaction chips.

If chips of different thickness were machined without re-zeroing the tooling, the depth of the milled chambers would vary, causing the resulting reaction chamber fill volumes to range from 0.8 µl to 1.3 µl. To correct for this, each batch of chips was measured and sorted by thickness, and the machine tooling was then re-zeroed to accurately account for the thickness of each batch.

Chip Alignment

In addition to accurate machining depth, a repeatable process for aligning the reaction chambers to reference features on the chip was developed. The prototype open-loop PCR device discussed in Chapter 3 used a mechanism consisting of 3 kinematic constraints to position the chamber relative to two edges of the chip and a leaf spring to provide the nesting force (Figure 12). After assessing the performance of this system several drawbacks were noted in this particular constraining mechanism. The repeatability depended upon the accurate placement of milled features on chips relative to

two sides. This meant that the CNC milling machine tools had to be zeroed to the edge of the fixture in *exactly* the same way each time. Also, the laser-cutting process creates a slight bevel on the edge of the chips. Depending upon how the chips were oriented in the milling fixture, the features could shift slightly to one side or the other. To eliminate these sources of error, two alignment pins were incorporated into the device and two alignment holes were machined into the chips. Because these holes were machined at the same time that the chamber was machined, the chamber would be located in the same place relative to the alignment holes, and the repeatability of this process is only limited by the repeatability of the CNC milling machine, which is within 6 μm (Figure 32).

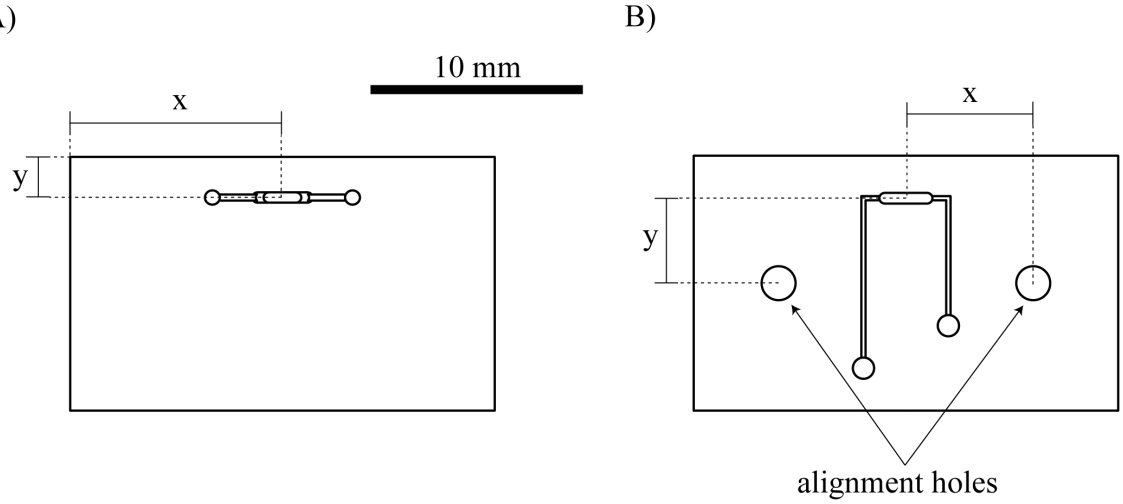

Figure 32: A) Microchip features referenced off of two edges of the chip increase variability in chamber placement. B) Microchip features referenced to two alignment holes allow for precise, repeatable chamber placement relative to alignment holes.

The bonding fixture incorporated these alignment pins as well, to ensure that the holes would not distort during the thermal bonding process.

Chip Bonding

After milling, chips were cleaned in a 3-stage process that consisted of 1) rinsing with isopropyl alcohol, 2) rinsing with deionized water, and 3) 18 minutes in an ultrasonic cleaner. After cleaning, chips were blown dry with compressed nitrogen. It was found that thermally bonding two layers of 1.50 mm acrylic together was the best

way to fabricate disposable reaction chips capable of withstanding the temperatures (95 °C) and pressures (40 psig) necessary for PCR (Figure 33).

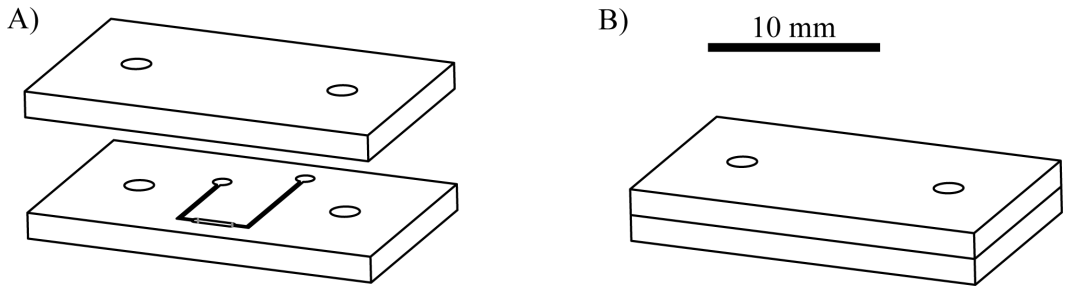

Figure 33: PCR microchips were fabricated from A) two pieces of 1.75 mm PMMA that were B) thermally bonded together.

Similar to developing repeatable machining techniques, a process for repeatable bonding had to be developed as well. Chips were bonded between two polished copper plates that were machined with alignment pins for aligning the two halves of the chip and threaded holes for bolts to provide the necessary clamping force. They were polished to a mirror finish to ensure the chips would be optically clear, a necessary requirement for real-time fluorescence. The plates were set on a hotplate and bolts tightened to 40 in-oz. The hotplate was then heated to 165 °C for 40 minutes. After 16 minutes of bonding time, the bolts were re-tightened to 36 in-oz. The temperatures, forces, and time for the bonding process were determined empirically to ensure a strong bond between the two layers of acrylic without significantly deforming any of the milled features.

Repeatability of Thermal Bonding Process

If the thermal bonding process was not repeatable, such that the bonding force, temperature, and bonding time varied significantly for different batches of chips, the alignment of the different features on the chips would shift relative to each other, preventing identical fill volumes and causing misalignment of the reaction chamber under the laser. To provide a repeatable bonding force, a torque screwdriver (Seekonk Precision Tools) was used to tighten the screws on the bonding fixture to ± 2 in-oz. For accurate bonding temperatures, a hotplate with digital readout to ± 5 °C was chosen

(Corning) and the bonding time was controlled via a digital timer with a resolution of ± 1 second (Woods). After bonding, the alignment of chip features was checked on a microscope and feature variation was found to be within ±15 μm for 10 batches of chips.

Chip Filling

While PMMA is easily machinable and thermally bondable, as well as able to withstand the temperatures and pressures necessary for PCR, it does not have the biocompatibility of other materials and has been known to inhibit PCR reactions. This inhibition of reactions has been shown to correlate to both the material properties and surface area-to-volume ratio of the device [56]. In addition to decreasing reaction efficiency, the fill channels of the reaction chip that were not being irradiated by the laser but still filled with PCR solution acted as dead volume since it was not being amplified. Dead volume dilutes the final PCR product and can inhibit the reaction by forming primer-dimers in the fill channels. With the current chip geometry, dead volume accounted for roughly 50% of the total fill volume of the chip.

Mineral Oil Filling

To reduce the amount of dead volume in the chip, mineral oil was flowed in both before and after the sample to occupy the fill channels of the chip during the reaction. This allowed for the sample to be confined to the reaction chamber, thus eliminating the dead volume (Figure 34).

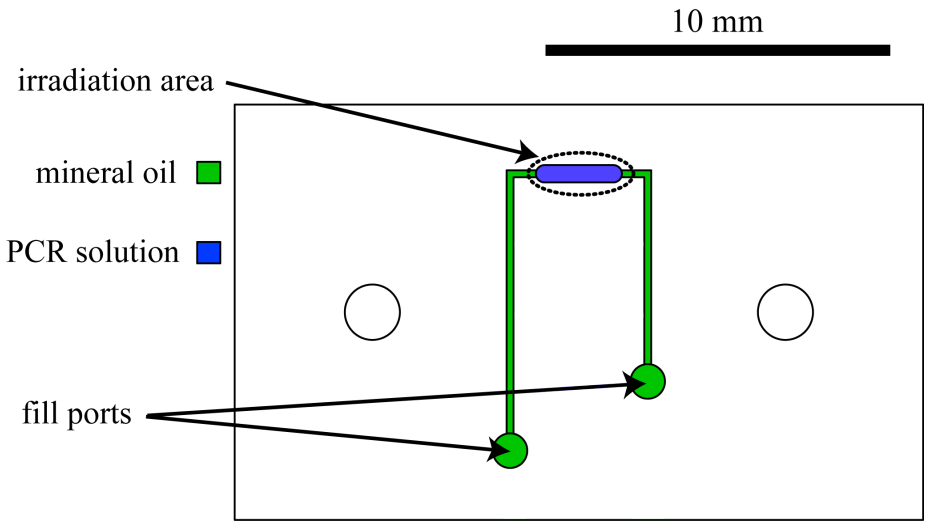

Figure 34: To reduce dead volume and increase amplification efficiency in PCR microchip, mineral oil was flowed in before and after the PCR solution so the PCR solution was confined to the area being irradiated by the laser.

At the completion of the reaction, the oil and PCR reaction was transferred into a small polypropylene PCR tube. Because mineral oil is hydrophobic, it separates from the PCR reaction in the tube and allows for just the PCR product to be extracted for off-line product quantification. In addition, the mineral oil flowed in before the PCR reaction coated the walls of the PMMA chip, thus encasing the reaction entirely in mineral oil and decreasing the absorption of nucleic acids and Taq polymerase onto the chamber walls. This significantly inhibited the detrimental effects of material properties and surface area-to-volume ratio that has plagued many micro-PCR devices.

CHAPTER 6

DESIGN OF SYSTEM

The incorporation of the aforementioned improvements resulted in the addition of a water-cooled copper environmental chamber to encase the PMMA chip, alignment pins and a pressurization system for the chip, as well as a water-cooled heat sink on top of the laser diode. The system was mounted on top of an inverted microscope to enable fluorescence imaging of the chamber for real-time detection purposes. The entire system is shown below (Figure 35).

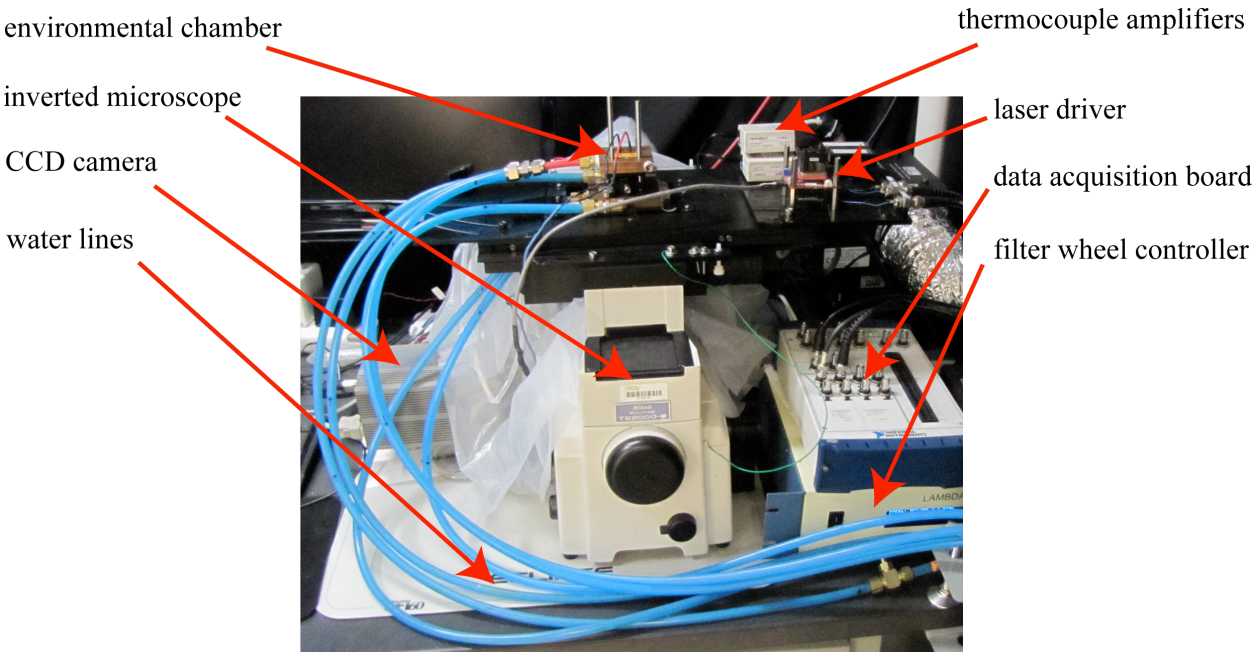

Figure 35: Overview of real-time PCR system. The environmental chamber and laser components were mounted on top of an inverted microscope to allow for imaging of the chamber during PCR.

Environmental Chamber

The copper environmental chamber represented the most significant update to the system. The functional requirements for the environmental chamber were:

1. Encase the reaction chip
2. Have a large thermal mass to validate the constant boundary condition assumption
3. Allow the top of the chamber to be irradiated by the laser
4. Bottom of chamber to be optically accessible for microscope imaging
5. Simple and fast chip loading and unloading process
6. Pressurized reaction chamber
7. Accurate and repeatable alignment of chip
8. Accurate and repeatable alignment of laser diode
9. Must be mountable and able to fit into 11 cm x 16 cm opening on microscope stage
10. PCR reaction chamber must remain within working distance of objective (15.7 mm)

The resulting design consisted of two 1/2 inch thick copper plates that were each machined to 80 mm x 80 mm. The bottom plate had three passages bored into the side. The outer two passages were designed as the water cooling passages and drilled on an angle to intersect at the far side of the chamber (Figure 36). The center passage was designed to deliver the 40 psig nitrogen to the fill ports of the chip and enable the chamber to remain pressurized during device operation. These pressurization ports were machined with slots for rubber O-rings to seal the chip against the plate and prevent leakage during operation. An 8 mm hole was drilled through the center of the plate,

which coincided with the center of the reaction chamber and allowed the chamber to be imaged. In addition, a recess with two alignment pins was created in the center of the plate. The recess ensured that the sides of the chip would also maintain a constant temperature and the alignment pins ensured accurate and repeatable placement of the chips in the device. The upper plate had one cooling passage drilled through. This passage was drilled offset from the center and unlike the lower plate with intersecting passages, this passage went straight through (Figure 36). An 8 mm hole was drilled through the center to allow the top of the chamber to be irradiated, and holes were drilled and tapped to allow the laser cage rod assembly to be mounted to the top plate.

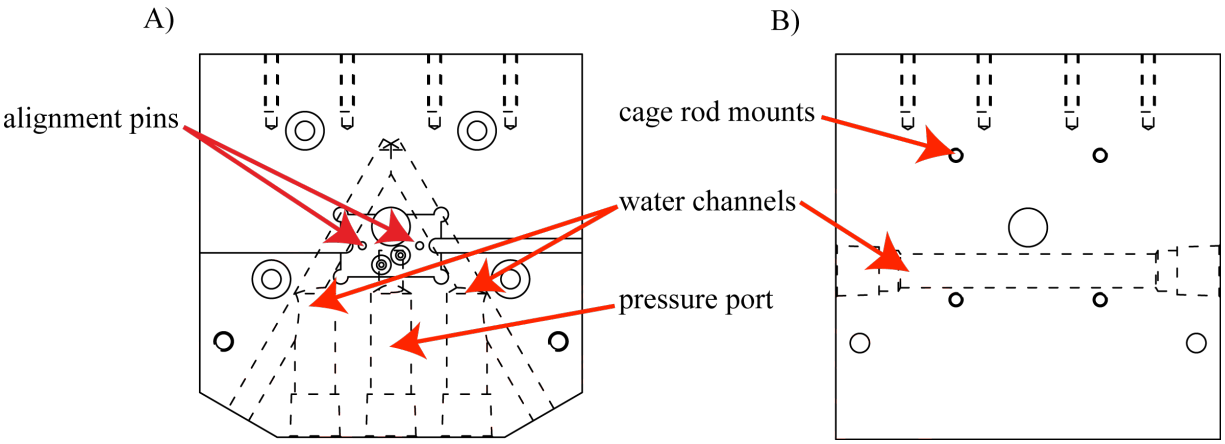

Figure 36: Drawings of A) bottom and B) top plate of environmental chamber. Internal water cooling passages and pressure ports are represented by dashed lines. Pins for aligning the chip were added to the bottom plate and holes to mount the laser cage rod assembly were located in the top plate.

To allow the plates to be separated for chip placement and removal but also maintain alignment between the two plates, a hinge was added to one side and holes drilled for two thumb screws on the other. The hinge allowed for only rotational movement between the two plates and the thumb screws, when tightened, provided a downward force on the top plate that seated the reaction chip against the rubber O-rings in the bottom plate to maintain 40 psig pressure in the chamber (Figure 37).

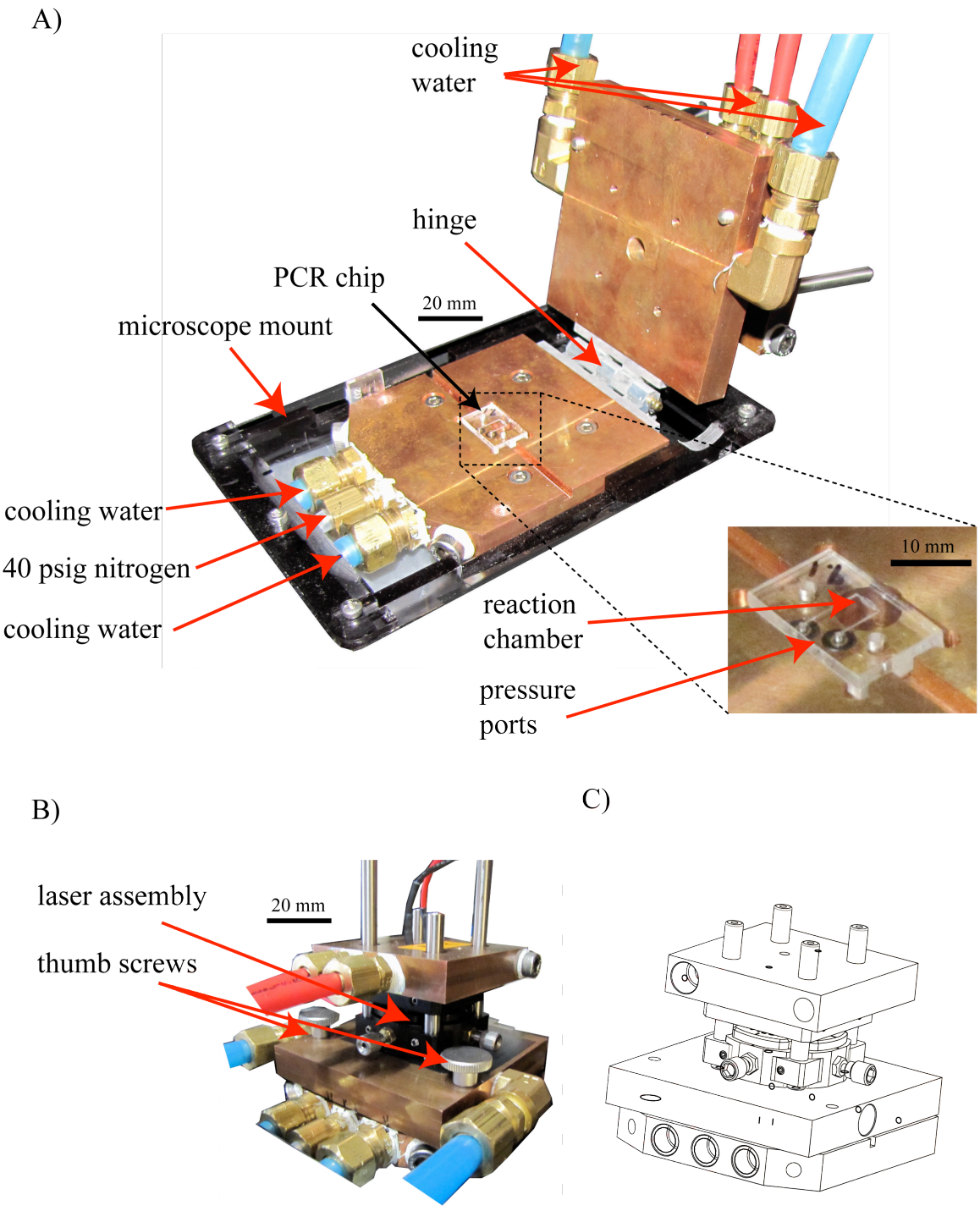

Figure 37: Layout of environmental chamber in A) open and B) closed positions as well as C) CAD drawing of system.

A constant temperature water bath with pump supplies the cooling water to the system. Manifolds were connected to the inlet and outlet of the pump and polypropylene tubing was used to run the water to each of the three heat sinks individually. Needle valves were located upstream of the components so the flow-rate to each component could be regulated. A schematic of the cooling system is shown in Figure 38.

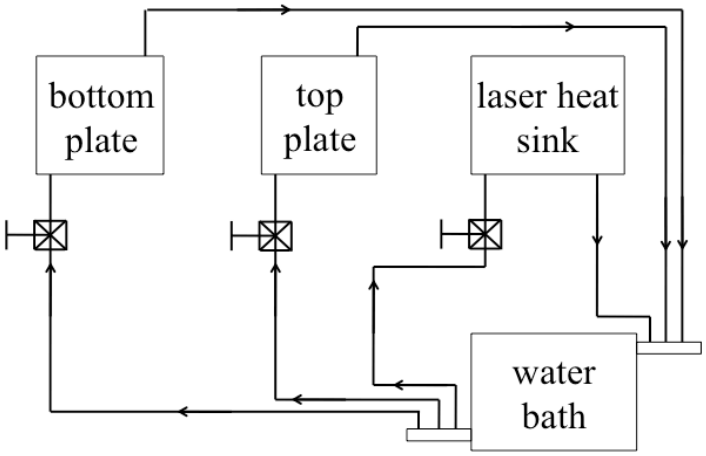

Figure 38: Schematic of cooling system.

Laser Assembly

The laser assembly consists of a 1450 nm infrared laser diode, aspherical collimating lens mounted in an x-y translational mount, and a water cooled copper heat sink mounted on top of the diode. To align the laser focal spot to the chamber, an empty chip was placed in the device with a piece of toner paper secured to the top. The laser was held at full power for 10 seconds and a hole corresponding to the focal spot of the laser was burned into the toner paper. The laser was turned off, chip removed, and the alignment of the focal spot to the chamber was checked under a microscope. If misaligned, the x-y translational mount was adjusted and the process continued until the focal spot was located directly over the reaction chamber.

Laser power output was regulated by the voltage sent to the laser driver. Using Labview we created software for analog open-loop laser driving voltage control. The

input is a simple text file containing a column of 0.10 second hold times and a corresponding column of drive voltages. The program reads through each line of the file, holding the laser driver at the specified voltage for the specified time. Once complete, the drive voltages returns to 0 and the program shuts off.

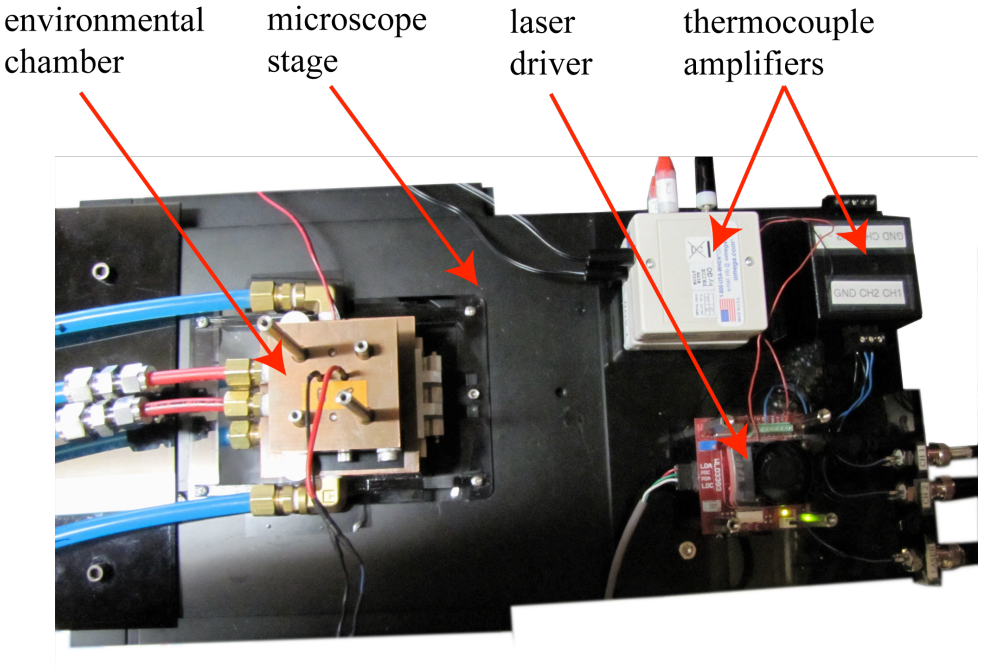

Figure 39: Top view of the layout of environmental chamber and laser components on microscope stage.

Microscope imagining and data acquisition assembly

The laser and environmental chamber assemblies were mounted on top of a Nikon Eclipse TE-2000E inverted microscope. A Sutter Lambda LS xenon arc lamp was used for the excitation light and filtered through a 480/20 nm bandpass filter. The emission light was filtered through a 520/20 nm bandpass filter and a Roper Scientific Cascade CCD camera was used to record images of the reaction chamber. The chamber was imaged through a 4x/0.2 N.A. Nikon objective. Images were gathered using NIS Elements BR software and post-processed via a MATLAB algorithm to identify the regions of intensity. A 3 mm thick water filter was added directly above the microscope

objective to absorb any stray infrared radiation and prevent it from damaging the microscope optics (Figure 40).

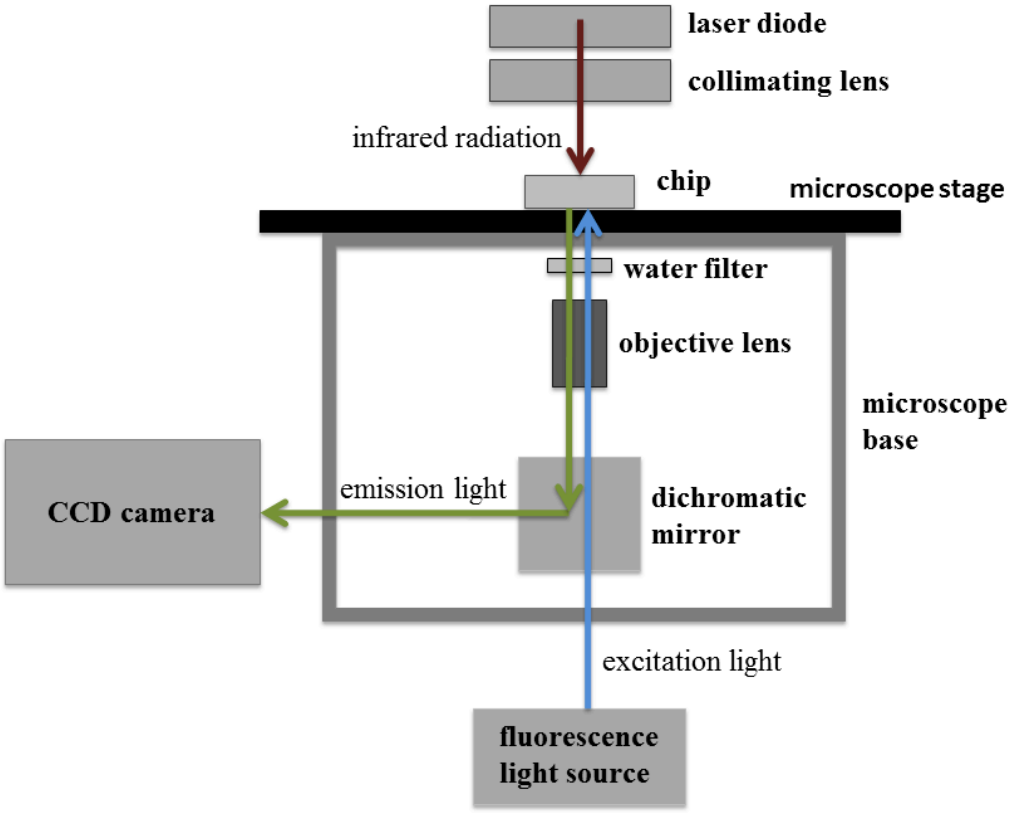

Figure 40: Schematic of microscope showing paths for excitation and emission light. The laser system was mounted on the stage facing down and a water filter used to prevent stray radiation from damaging the optical components.

Mechanical and Thermal Repeatability

After the components were fabricated and installed, the repeatability of the system was assessed. To measure the repeatability of the alignment pins, an empty reaction chip was placed in the device, and imaged with the microscope. The position of the chamber was recorded on the screen, and the process repeated 10 times. The average variation in chip placement was 5 μm, or 1 % of the reaction chamber width.

The focal spot of the laser diode was aligned over the chamber using sheets of toner paper as previously mentioned. This process, once properly adjusted, does not have

to be repeated during normal operation of the machine. However, to assess the combined repeatability of the hinge in aligning the top plate to the bottom plate of the environmental chamber and the alignment pins in aligning the chips to the bottom plate, 10 squares of toner paper were prepared and fixed on top of 10 chips. Each chip was then placed in the device and the laser power turned on full for 10 seconds. The chip was removed, and the focal spot was imaged with a microscope to check for alignment and all 10 focal spots were found to be consistently aligned over the chambers.

To assess the thermal stability of the environmental chamber, a reaction chip was filled and placed in the device with the laser diode off but with water flowing through the environmental chamber. The temperature of the reaction chamber was monitored and over a 1 minute time, the standard deviation in temperature was found to be 0.076 °C.

CHAPTER 7

RESULTS

The combination of thermal and chip manufacturing improvements greatly increased the temperature stability and repeatability of the system. We found the temperature variation during reverse-transcription, the annealing step, and the extension step to be σ_{RT} = 0.076 °C, σ_a = 0.18 °C, and σ_e = 0.15 °C respectively with average heating and cooling rates of 3.3 °C and 3.86 °C. This temperature stability is comparable to those reported by other closed-loop micro PCR systems. One such system, by Angione et al., recently reported temperature variations of σ_{RT} = 0.8 °C, σa = 0.1 °C, and σ_e = 1.3 °C during the reverse-transcription, annealing, and extension steps and heating and cooling rates of 1.6 °C and 1.8 °C [57].

To quantify the impact of these improvements on PCR yield, real-time amplifications of both DNA and RNA were performed. The system performance would be assessed in terms of PCR product yield and repeatability of real-time fluorescence curves.

PCR Amplifications

PCR Protocol

After thermal bonding, chips were rinsed with deionized water, dried with compressed nitrogen, numbered, and placed in a sterile Petri dish. A 500 bp amplicon of λ phage DNA (USB) was chosen as the target to be amplified and the following primer set 5′-GATGAGTTCGTGTTCGTACAACTGG-3′ and 5′-GGTTATCGAAATCAGCCACAGCGCC-3′ was used. Primers were obtained from eurofins, re-suspended and diluted into 20 mM aliquots according to the manufacturer's protocol. Bioneer AccuPower PCR PreMix tubes were used for the reaction premix and SYBR Green I dye (Lonza) was used for real-time detection. BSA (USB) was added to

the reaction to lessen the Taq polymerase absorption to the walls of the chamber. The reaction was prepared according to the following protocol: 11 µl H_2O, 6.0 µl BSA (1 µg/µl), 0.6 µl SYBR Green I (10x), 0.4 µl forward and reverse primers (20 mM), 2.0 µl DNA (varying concentrations) were added into one 20 µl PCR premix tube. A 5 µl aliquot was taken, covered by 15 µl of mineral oil (Fischer Scientific), and run on a conventional thermocycler (BioRad, MJ Mini) for 40 cycles. Each cycle consisted of 95 °C for 30 s, 68 °C for 60 s, and 72 °C for 60 s. In addition, a 5 minute, 95 °C initial denaturation step was done at the beginning of cycling and a 2 minute, 72 °C final extension at the end.

The remaining PCR solution was divided up into 2 µl aliquots, one for each reaction to be performed. The water bath, CCD camera, laser driver, and xenon lamp were switched on and allowed to run for 30 minutes. The constant temperature water bath was set at 42.8 °C. After the 30 minute warm-up, a calibration chip was placed in the machine and run through one PCR program to verify the entire system was functioning properly. Pipettes were then filled in a 3-stage process: 1.53 µl of mineral oil, followed by 0.94 µl of PCR solution, followed by another 1.53 µl of mineral oil. The solution was flowed into a clean PCR microchip, taking care to ensure the PCR solution was centered in the reaction chamber, placed in the device and run through 30 PCR cycles. Each cycle consisted of 93 °C for 10 s, 68 °C for 20 s, and 72 °C for 20 s. In addition, a 60 s initial denaturation was done at the beginning of cycling (Figure 41).

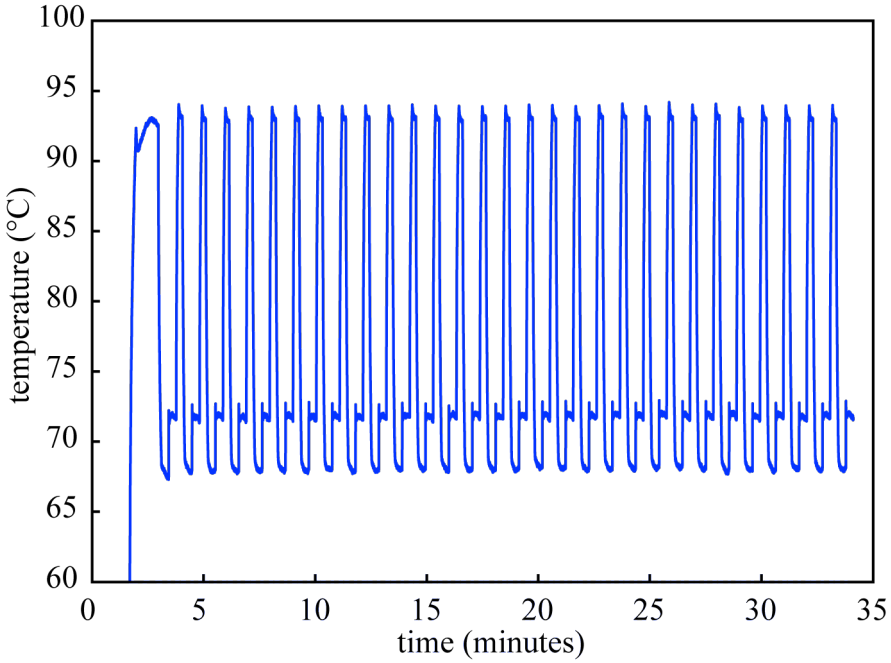

Figure 41: Temperature as a function of time for 30 PCR cycles with a 500 bp segment of λ phage DNA as the amplicon. The system is calibrated by creating an optimized laser power profiles, measuring the temperature response, and then adjusting the power profile as needed. Once created, the same open-loop program can be run multiple times with no need for re-calibration between runs.

Fluorescence Measurements

Fluorescence measurements were taken during the extension phase of every PCR cycle. To avoid photobleaching of the SYBR Green dye due to prolonged exposure to the excitation light, camera exposure time was limited to 2 seconds and images were taken after the first 17 seconds of each extension phase. After the PCR run was complete, the fluorescence images were saved and post-processed to determine the change in fluorescence intensity. An algorithm was written in MATLAB that calculated the average intensity of a user-defined region of interest. The same region of interest was used for all images, and the algorithm output was a vector of 30 average intensities over the region of interest. The vector was then normalized so all values ranged from 0 to 1.

Standard Curve Construction

The process was repeated 3 times for a series of 4 - 10x dilutions of DNA. The normalized fluorescence intensities for each dilution were averaged, and the results for all 4 dilutions (each averaged from n = 3 runs) plotted together (Figure 42).

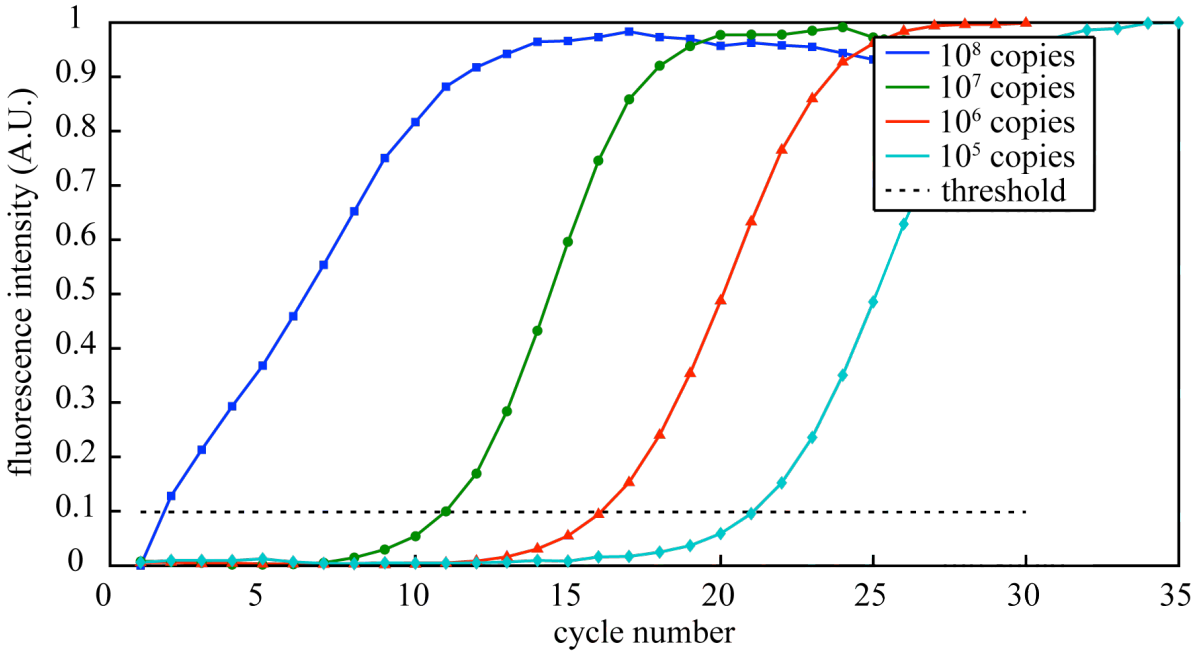

Figure 42: Fluorescence intensity of a PCR sample as a function of cycle number. As the concentration of DNA increases, the fluorescence intensity of the sample increases. Reactions with fewer starting copies of DNA take more cycles before the fluorescence intensity crosses the detection threshold of the system.

The fluorescence threshold was taken as 30 times the standard deviation of the first 6 PCR cycles, and from this the average cycle threshold value for each dilution was determined. The fluorescence intensities of the highest starting concentrations began to exponentially increase immediately; therefore no accurate cycle threshold value could be determined from the highest concentration. For the remaining 3, the base 10 logarithms of the starting copy numbers were plotted against the cycle threshold values, and a linear

regression fit was performed. The coefficient of determination from this regression analysis was $R^2 = 0.9933$, indicating the linear model fit the data well (Figure 43).

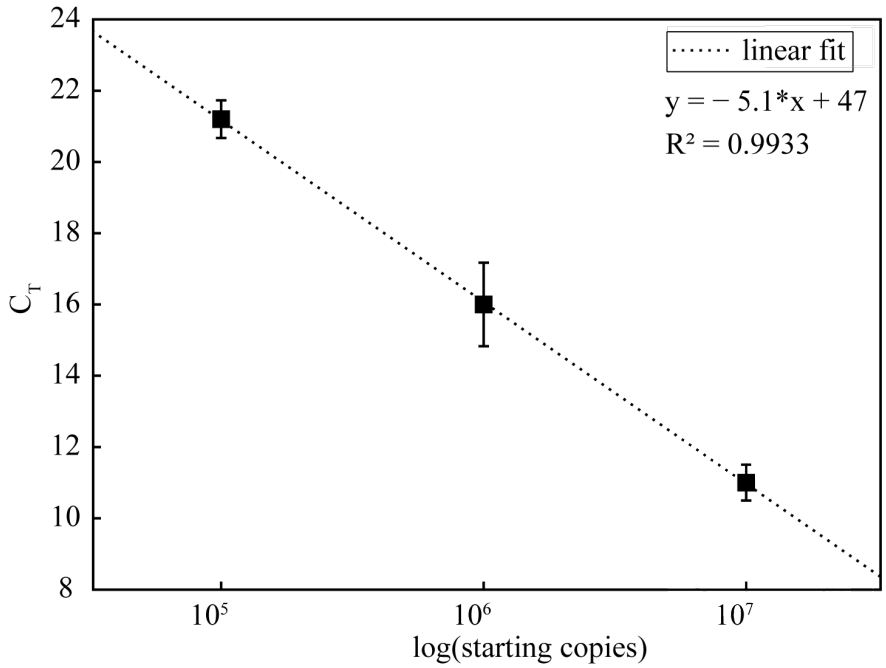

Figure 43: Cycle threshold as a function of starting copies for 3 dilutions of lambda phage DNA. The relationship between the log of the starting copy number and cycle threshold value is a straight line, as shown by the linear regression fit.

The efficiency of the open-loop PCR system was calculated from the slope of the standard curve as:

$$E = 100*(10^{-1/k} - 1) \qquad \textbf{(Eq. 3)}$$

where E is the efficiency of the system and k is the slope of the linear fit [58]. The efficiency of the device was 57%.

Bioanalyzer Results – Comparison to Thermocycler

The PCR product from both the laser device and conventional thermocycler controls was evaluated with microchannel electrophoresis separation (Agilent,

Bioanalyzer) to determine both the base-pair length and final concentration of PCR product (Figure 44).

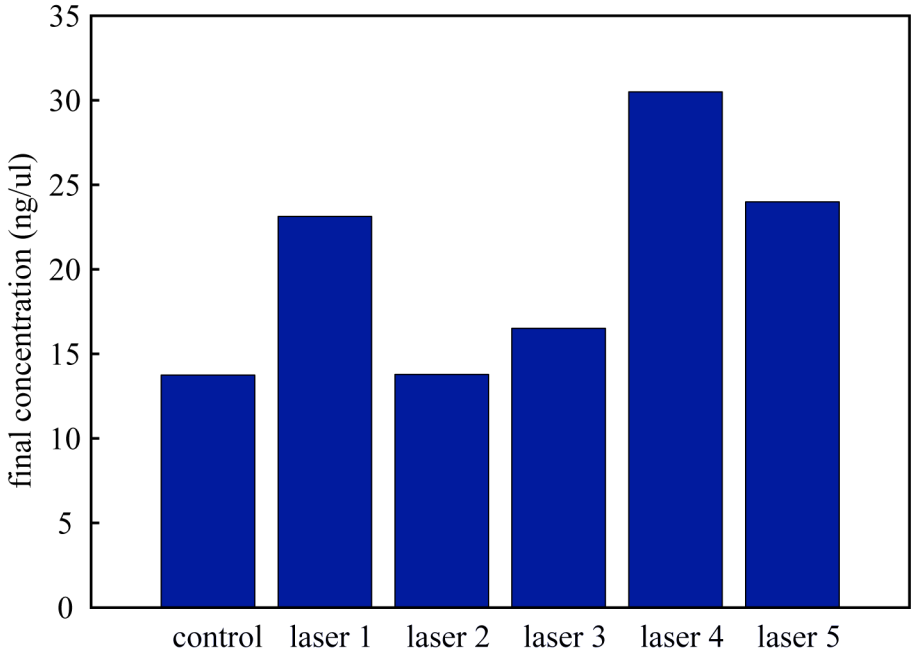

Figure 44: Final concentrations of PCR product for a thermocycler control, labeled as control, and amplifications performed with the open-loop laser system, labeled as laser 1 - 5. The final concentrations of PCR product from both systems were not statistically different, indicating the laser system is as efficient as current techniques.

A two-sample t-test was used to determine if the average final concentration of PCR product from the five open-loop system amplifications was statistically different from the thermocycler control. A null hypothesis that the two means were equal was assumed. The result of the test was a p value of 0.5823 and an h value of 0, indicating a failure to reject the null hypothesis at the 1% significance level. These results indicated that the laser system produced a statistically similar PCR final concentration to the thermocycler controls.

Reverse Transcription Amplifications

Reverse Transcription Protocol

The housekeeping gene GAPDH was chosen as the target to be amplified from samples of purified mouse embryonic stem cell RNA using the following primer set 5′-GCCTTCCGTGTTCCTACC-3′ and 5′-GCCTGCTTCACCACCTTC-3′. Primers were obtained from eurofins, re-suspended and diluted into 10 mM aliquots according to the manufacturer's protocol. Bioneer AccuPower one-step RT-PCR PreMix tubes were used for the reaction premix and SYBR Green I dye (Lonza) was used for real-time detection. BSA (USB) was added to the reaction to lessen the Taq polymerase absorption to the walls of the chamber. The reaction was prepared according to the following protocol: 14.1 µl H_2O, 3.0 µl BSA (1 µg/µl), 0.40 µl SYBR Green I (10x), 0.75 µl forward primer (10 mM), 0.75 µl reverse primer (10 mM), and 1.0 µl RNA (109 ng/µl) were added into one 20 µl RT-PCR premix tube. A 5 µl aliquot was taken, covered by 15 µl of mineral oil (Fischer Scientific), and run on a conventional thermocycler (BioRad, MJ Mini). The sample was first held at 42 °C for 60 minutes for the reverse transcription process followed by 40 PCR cycles. Each cycle consisted of 94 °C for 10 s, 56 °C for 30 s, and 72 °C for 30 s. In addition, a 5 minute, 94 °C initial denaturation step was done at the beginning of cycling.

The remaining PCR solution was divided up into 2 µl aliquots, one for each reaction to be performed. The water bath, CCD camera, laser driver, and xenon lamp were switched on and allowed to warm up for 30 minutes. The temperature of the water bath was set for 42.8 °C which created a 42 °C temperature in the reaction chamber, the optimal temperature for reverse transcription. Pipettes were filled in a 3-stage process: 1.53 µl of mineral oil, followed by 0.94 µl of PCR solution, followed by another 1.53 µl of mineral oil (Figure 34). The solution was flowed into a clean PCR microchip, taking care to ensure the PCR solution was centered in the reaction chamber, and then placed in the device. The chip remained in the device for 30 minutes with the laser off to allow the reverse transcription to occur and then run through 30 PCR cycles. Each cycle consisted of 93 °C for 10 s, 56 °C for 20 s, and 72 °C for 20 s. In addition, a 5 minute, 93 °C initial

denaturation was done at the beginning of cycling to inactivate the reverse transcriptase and denature the cDNA (Figure 45).

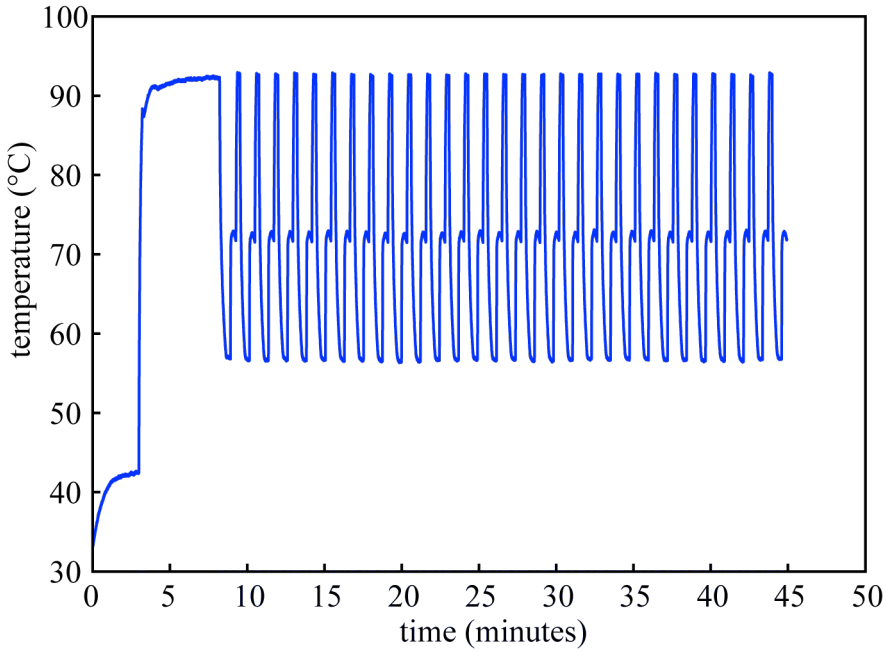

Figure 45: Temperature as a function of time for 30 PCR cycles with the gene GAPDH, a 100 bp segment of RNA, as the amplicon. The system is calibrated by creating an optimized laser power profiles, measuring the temperature response, and then adjusting the power profile as needed. Once created, the same open-loop program can be run multiple times with no need for re-calibration between runs.

Heating and Fluorescence Measurements

Fluorescence measurements were taken during the extension phase of every PCR cycle. Camera exposure time was set to 2 seconds and images were taken after the first 17 seconds of each extension phase. After the PCR run was complete, the fluorescence images were saved and post-processed to determine the change in fluorescence intensity. The data was post-processed in MATLAB and the intensities were normalized relative to the fluorescence intensity of the last cycle. In addition, all values below the initial intensity level were set to 0 (Figure 46).

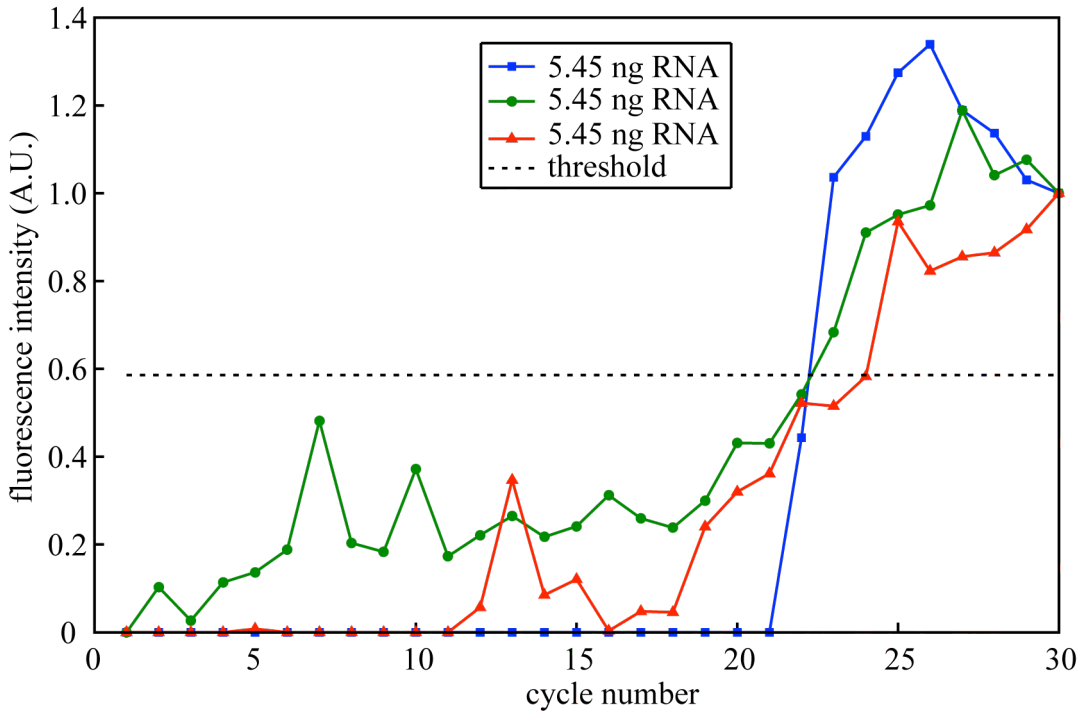

Figure 46: Fluorescence intensity of a PCR sample as a function of cycle number for three amplifications of the gene GAPDH with identical amounts of RNA. As the concentration of cDNA increases, the fluorescence intensity of the sample increases.

Bioanalyzer Results – Comparison to Thermocycler

The PCR product from both the laser device and conventional thermocycler controls was evaluated with microchannel electrophoresis separation (Agilent, Bioanalyzer) to determine both the base-pair length and final concentration of PCR product. The final concentrations of PCR product were similar for both systems, indicating the laser system is as efficient as current techniques (Figure 47).

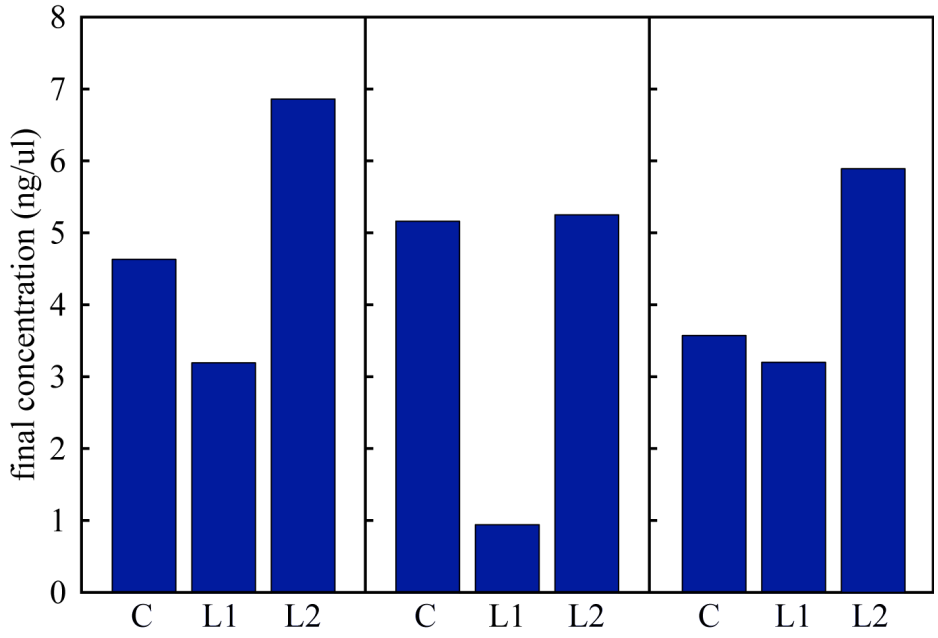

Figure 47: Final concentrations of PCR product for thermocycler controls, labeled as C, and amplifications performed with the open-loop laser system, labeled as L. The final concentrations of PCR product from both systems were not statistically different, indicating the laser system is as efficient as current techniques.

Statistical Analysis

A two-sample t-test was again used to determine if the average final concentration from the three thermocycler control amplifications was statistically different from the six amplifications done with the open-loop system. A hull hypothesis that the two sample means were equal was assumed and evaluated at a 1% significance level. The results indicated a failure to reject the null hypothesis at the 1% significance level and a p value of 0.8672 so the average PCR product from the thermocycler and open-loop system were statistically similar.

CHAPTER 8

CONCLUSIONS AND FUTURE WORK

Since the 1990's, the field of micro PCR has been steadily advancing. Many researchers have focused on developing systems that can perform gene expression measurements on hundreds cells at once, or on thousands of genes of interest, or with sample-in answer-out capability. However the fabrication cost, set-up time, or difficulty of use has prohibited these instruments from scaling easily in the time domain. In this thesis we have described the design, fabrication, and testing of two iterations of devices for performing micro PCR with open-loop control. Combining the benefits of micro PCR with the speed and simplicity of open-loop control is a promising way to scale gene expression measurements in the time domain. By implementing an optimized power profile, environmental control, a pressurized reaction chamber, and refined chip manufacturing, bonding, and filling techniques, we have created a system that can amplify targets of DNA or RNA with the same efficiency as conventional thermocyclers, 1/25 the volume, and in ½ to 1/3 the time a conventional machine takes. In addition, the implementation of fluorescence detection and successful construction of a standards curve for λ phage DNA has enabled sample concentrations to be quantified in real-time.

Future Work

There is still work to be done to create a system fully capable of measuring gene expression at a high temporal frequency. This system used purified RNA as the starting point. However, further upstream processing steps such as cell extraction, lysis, and RNA purification need to be integrated into the device in order to decrease the labor and sample handling involved. Also, an automated system to clean or replace reaction chips between runs is essential when measuring gene expression every hour over multiple days. Further work involves better characterization of the laser power profiles. Currently, the profile irradiating the reaction chamber has a Gaussian profile, creating uneven heating in

the chamber. Irradiating the chamber with a flat, even profile would further increase the efficiency of the system to possibly exceed the efficiency of conventional thermocyclers.

Alternative Applications

While high-frequency gene expression measurement is one future application for the device, another would be as a point-of-care device in developing countries. To use the device as a compact, nucleic acid amplification device, Peltier heaters could replace the water-cooled environmental chamber to reduce the size of the device. In addition, the laser power could be split evenly over multiple channels, allowing for simultaneous amplifications of multiple samples. The simple chip filling and loading technique is unique among microfluidic devices, and open-loop control combined with inexpensive, disposable PMMA chips significantly increases the practicality of micro PCR technologies.

REFERENCES

[1] K. Mullis, Faltoona, F., Scharf, S., Saiki, R., Horn, G., Erlich, H., "Specific enzymatic amplification of DNA in vitro: the polymerase chain reaction," *Cold Spring Harbor Symp Quant Biol,* vol. 51, pp. 263 - 273, 1986.

[2] M. Kubista, Andrade, J., Bengtsson, M., Forootan, A., Jonak, J., Lind, K., Sindelka, R., Sjoback, R., Sjogreen, B., Strombom, L., Stahlberg, A., Zoric, N., "The real-time polymerase chain reaction," *Molecular Aspects of Medicine,* vol. 27, pp. 95-125, 2006.

[3] Y. Zhang, Ozdemir, P., "Microfluidic DNA amplification - A review," *Analytica Chimica Acta,* vol. 638, pp. 115-125, 2009.

[4] D. Lee, Chen, P., Lee, G., "The evolution of real-time PCR machines to real-time PCR chips," *Biosensors and Bioelectronics,* vol. 25, pp. 1820-1824, 2010.

[5] Y. H. Kim, Yang, I., Bae, Y.S., Park, S.R., "Performance evaluation of thermal cyclers for PCR in a rapid cycling condition," *Biotechniques,* vol. 44, pp. 495 - 505, 2008.

[6] I. Yang, Kim, Y., Byun, J., Park, S., "Use of multiplex polymerase chain reactions to indicate the accuracy of the annealing temperature of thermal cycling," *Analytical Biochemistry,* vol. 338, pp. 192-200, 2004.

[7] C. T. Wittwer, Ririe, K.M., Andrew, R.V., David, D.A., Gundry, R.A., Balis, U.J., "The LightCycler(TM) a microvolume multisample fluorimeter with rapid temperature control," *Biotechniques,* vol. 22, pp. 176 - 181, 1997.

[8] S. Park, Zhang, Y., Lin, S., Wang, T., Yang, S., "Advances in microfluidic PCR for point-of-care infectous disease diagnostics," *Biotechnology Advances,* vol. 29, pp. 830-839, 2011.

[9] M. Arya, Shergill, I., Williamson, M., Gommersall, L., Arya, N., Patel, H., "Basic principles of real-time quantitative PCR," *Expert Review of Molecular Diagnostics,* vol. 5, pp. 209-219, 2005.

[10] R. Higuchi, Fockler, C., Dollinger, G., Watson, R., "Kinetic PCR analysis: real-time monitoring of DNA amplification reactions," *Biotechnology,* vol. 11, pp. 1026 - 1030, 1993.

[11] S. Itzkovitz, van Oudenaarden, A., "Validating transcripts with probes and imaging technology," *Nature Methods Supplement,* vol. 8, pp. 512 - 519, 2011.

[12] J. H. Malone, Oliver, B., "Microarrays, deep sequencing and the true measure of the transcriptome," *BMC Biology,* vol. 9, pp. 1-9, 2011.

[13] M. Schena, Shalon, D., Davis, R.W., Brown, P.O., "Quantitative monitoring of gene expression patterns with a complementary DNA microarray," *Science,* vol. 270, pp. 467 - 470, 1995.

[14] A. Dahl, Sultan, M., Jung, A., Schwartz, R., Lange, M., Steinwand, M., Livak, K., Lehrach, H., Nyarsik, L., "Quantitative PCR based expression analysis on a nanoliter scale using polymer nano-well chips," *Biomedical Microdevices,* vol. 9, pp. 307-314, 2007.

[15] J. Hipp, Hipp, J., Atala, A., Soker, S., "Functional Genomics: New Insights into the 'Function' of Low Levels of Gene Expression in Stem Cells," *Current Genomics,* vol. 11, pp. 354-359, 2010.

[16] Y. Toh, Blagovic, K., Voldman, J., "Advancing stem cell research with microtechnologies: opportunities and challenges," *Integrative Biology,* vol. 2, pp. 305-325, 2010.
[17] N. Yosef, Regev, A., "Impulse control: Temporal dynamics in gene transcription," *Cell Science at a Glance,* vol. 144, pp. 886 - 896, 2011.
[18] A. Stahlberg, Bengtsson, M., "Single-cell gene expression profiling using reverse transcription quantitative real-time PCR," *Methods,* vol. 50, pp. 282 - 288, 2010.
[19] J. McClellan, McDevitt, T., "Personal Communication - Laboratory techniques for measuring stem cell gene expression," ed. Atlanta, GA, 2011.
[20] C. Zhang, Xu, J., Ma, W., Zheng, W., "PCR microfluidic devices for DNA amplification," *Biotechnology Advances,* vol. 24, pp. 243-284, 2006.
[21] N. R. Beer, Hindson, B.J., Wheeler, E.K., Hall, S.B., Rose, K.A., Kennedy, I.M., Colston, B.W., "On-Chip, Real-Time, Single-Copy Polymerase Chain Reaction in Picoliter Droplets," *Analytical Chemistry,* vol. 79, pp. 8471 - 8475, 2007.
[22] M. Curcio, Roeraade, J., "Continuous Segmented-Flow Polymerase Chain Reaction for High-Throughput Miniaturized DNA Amplification," *Analytical Chemistry,* vol. 75, pp. 1-7, 2003.
[23] K. D. Dorfman, Chabert, M., Codarbox, J.-H., Rousseau, G., de Cremoux, P., Viovy, J.-L., "Contamination-Free Continuous Flow Microfluidic Polymerase Chain Reaction for Quantitiative and Clinical Applications," *Analytical Chemistry,* vol. 77, pp. 3700 - 3704, 2005.
[24] J. Khandurina, McKnight, T.E., Jacobson, S.C., Waters, L.C., Foote, R.S., Ramsey, J.M., "Integrated system for rapid PCR-based DNA analysis in microfluidic devices," *Analytical Chemistry,* vol. 72, pp. 2995 - 3000, 2000.
[25] Y. Matsubara, Kerman, K., Kobayashi, M., Yamamura, S., Morita, Y., Takamura, Y., Tamiya, E., "On-Chip Nanoliter-Volume Multiplex TaqMan Polymerase Chain Reaction from A Single Copy Based on Counting Fluorescence Released Microchambers," *Analytical Chemistry,* vol. 76, pp. 6434-6439, November 1, 2004 2004.
[26] H. Nagai, Murakami, Y., Yokoyama, K., Tamiya, E., "High-throughput PCR in silicon based microchamber array," *Biosensors and Bioelectronics,* vol. 16, pp. 1015 - 1019, 2001.
[27] M. Slyadnev, Lavrova, M., Erkin, M., Kazakov, V., Ganeev, A., "Development of a Multireactor Microfluidic System for the Determination of DNA Using Real-Time Polymerase Chain Reaction," *Journal of Analytical Chemistry,* vol. 63, pp. 192-198, 2008.
[28] C.-S. Liao, Lee, G.-B., Liu, H.-S., Hsieh, T.-M., Luo, C.-H., "Miniature RT-PCR system for diagnosis of RNAbased viruses," *Nucleic Acids Research,* vol. 33, p. e156, 2005.
[29] K.-Y. Lien, Lee, W.-C., Lei, H.-Y., Lee, G.-B., "Integrated reverse transcription polymerase chain reaction systems for virus detection," *Biosensors and Bioelectronics,* vol. 22, pp. 1739 - 1748, 2007.
[30] P. Liu, Seo, T.S., Beyor, N., Shin, K.-J., Scherer, J.R., Mathies, R.A., "Integrated portable polymerase chain reaction-capillary electrophoresis microsystem for rapid forensic short tandem repeat typing," *Analytical Chemistry,* vol. 79, pp. 1881 - 1889, 2007.

[31] B. Minqiang, Melvin, T., Ensell, G., Wilkinson, J., Evans, A., "Design and theoretical evaluation of a novel microfluidic device to be used for PCR," *J. Micromech. Microeng.,* vol. 13, p. S125, 2003.
[32] P. Neuzil, Zhang, C., Pipper, J., Oh, S., Zhou, L., "Ultra fast miniaturized real-time PCR: 40 cycles in less than six minutes," *Nucleic Acids Research,* vol. 34, p. e77, May 24, 2006 2006.
[33] M. A. Northrup, Benett, B., Hadley, D., Landre, P., Lehew, S., Richards, J., "A miniature analytical instrument for nucleic acids based on micromachined silicon reaction chambers," *Analytical Chemistry,* vol. 70, pp. 918 - 922, 1998.
[34] Z. Wang, Sekulvoic, A., Kutter, J.P., Bang, D.D., Wolff, A., "Towards a portable microchip system with integrated thermal control and polymer waveguides for real-time PCR," *Electrophoresis,* vol. 27, pp. 5051 - 5058, 2006.
[35] A. T. Wooley, Hadley, D., Landre, P., de Mello, A.J., Mathies, R.A., Northrup, M.A., "Functional integration of PCR amplification and capillary electrphoresis in a microfabricated DNA analysis device," *Analytical Chemistry,* vol. 68, pp. 4081 - 4086, 1996.
[36] Q. Xiang, Xu, B., Fu, R., Li, D., "Real Time PCR on Disposable PDMS Chip with a Miniaturized Thermal Cycler," *Biomedical Microdevices,* vol. 7, pp. 273-279, 2005.
[37] Q. B. Zou, Sridhar, U., Chen, Y., Singh, J., "Miniaturized, independently controllable multichamber thermal cycler," *IEEE Sensors J.,* vol. 3, pp. 774 - 780, 2003.
[38] M. Focke, Stumpf, F., Roth, G., Zengerle, R., von Stetten, F., "Centrifugal microfluidic system for primary amplification and secondary real-time PCR," *Lab on a Chip,* vol. 10, pp. 3210 - 3212, 2010.
[39] E. K. Wheeler, Benett, W., Stratton, P., Richards, J., Chen, A., Christian, A., "Convectively driven polymerase chain reaction thermal cycler," *Analytical Chemistry,* vol. 76, pp. 4011 - 4016, 2004.
[40] C. T. Wittwer, Fillmore, G.C., Garling, D.J., "Mimimizing the time required for DNA amplification by efficient heat transfer to small samples," *Analytical Biochemistry,* vol. 186, pp. 328 - 331, 1990.
[41] C. J. Easley, Karlinsey, J.M., Bienvenue, J.M., Legendre, L.A., Roper, M.G., Feldman, S.H., Landers, J.P., "A fully integrated microfluidic genetic analysis system with sample-in-answer-out capability," *Proceedings of the National Academy of Sciences,* vol. 103, pp. 19272 - 19277, 2006.
[42] A. Huhmer, Landers, J., "Noncontact infrared-mediated thermocycling for effective polymerase chain reaction amplification of dna in nanoliter volumes," *Analytical Chemistry,* vol. 72, pp. 5507-5512, 2000.
[43] R. P. Oda, Strausbauch, M.A., Huhmer, A.F.R., Borson, N., Jurrens, S.R., Craighead, J., "Infrared mediated thermocycling for ultrafast polymerase chain reaction amplification of DNA," *Analytical Chemistry,* vol. 70, pp. 4361 - 4368, 1998.
[44] H. Kim, Vishniakou, S., Faris, G., "Petri dish PCR: laser-heated reactions in nanoliter droplet arrays," *Lab on a Chip,* vol. 9, pp. 1230-1235, 2009.

[45] M. Slyandev, Tanaka, Y., Tokeshi, M., Kitamori, T., "Photothermal Temperature Control of a Chemical Reaction on a Microchip Using an Infrared Diode Laser," *Analytical Chemistry,* vol. 73, pp. 4037-4044, 2001.
[46] H. Terazono, Hattori, A., Takei, H., Takeda, K., Yasuda, K., "Development of 1480 nm photothermal high-speed real-time polymerase chain reaction system for rapid nucleotide recognition," *Japanese Journal of Applied Physics,* vol. 47, p. 5212, 2008.
[47] A. V. White, M., Petriv, O., Hamidi, M., Sikorski, D., Marra, M., Piret, J., Aparicio, S., Hansen, C., "High-throughput microfluidic single-cell RT-qPCR," *PNAS,* vol. 108, pp. 13999-14004, 2011.
[48] R. Zare, Kim, S., "Microfluidic Platforms for Single-Cell Analysis," *Annual Review of Biomedical Engineering,* vol. 12, pp. 187-201, 2010.
[49] Y. Zeng, Novak, R., Shuga, J., Smith, M., Mathies, R., "High-Performance Single Cell Genetic Analysis Using Microfluidic Emulsion Generator Arrays," *Analytical Chemistry,* vol. 82, pp. 3183-3190, 2010.
[50] J. Zhong, Chen, Y., Marcus, J., Scherer, A., Quake, S., Taylor, C., Weiner, L., "A microfluidic processor for gene expression profiling of single human embryonic stem cells," *Lab on a Chip,* vol. 8, pp. 68-74, 2007.
[51] J. Zhong, Feng, Y., Taylor, C., "Microfluidic Devices for Investigating Stem Cell Gene Regulation via Single-Cell Analysis," *Current Medicinal Chemistry,* vol. 15, pp. 2897-2900, 2008.
[52] C. Phaneuf, Pak, N., Forest, C., "Modeling radiative heating of liquids in microchip reaction chambers," *Sensors and Actuators,* vol. 167, pp. 531-536, 2011.
[53] A. A. Sodemann, Mayor, J.R., "Parametric investigation of precision in tool-workpiece conductivity touch-off method in micromilling," *Trans. N. Am. Manuf. Res. Inst. SME,* vol. 37, pp. 565 - 572, 2009.
[54] D. S. Lee, Park, S.H., Yang, H., Chung, K.H., Yoon, T.H., Kim, S.J., Kim, K., Kim, Y.T., "Bulk-micromachined submicroliter-volume PCR chip with very rapid thermal response and low power consumption," *Lab on a Chip,* vol. 4, pp. 401 - 407, 2004.
[55] H.-B. Liu, Gong, H.-Q., Ramalingam, N., Jiang, Y., Dai, C.-C., Hui. K. M., "Micro air bubble formation and its control during polymerase chain reaction (PCR) in polydimethylsiloxane (PDMS) microreactors," *Journal of Micromechanics and Microengineering,* vol. 17, pp. 2055 - 2064, 2007.
[56] C. Potrich, Lunelli, L., Forti, S., Vozzi, D., Pasquardini, L., Vanzetti, L., Pahciatichi, C., Anderle, M., Pederzolli, C., "Effect of materials for micro-electric-mechanical systems on PCR yield," *European Biophysicsl Journal,* vol. 39, pp. 979-986, 2010.
[57] S. Angione, Chauhan, A., Tripathi, A., "Real-Time Droplet DNA Amplification with a New Tablet Platform," *Analytical Chemistry,* vol. 84, pp. 2654-2661, 2012.
[58] R. G. Rutledge, Cote, C., "Mathematics of quantitative kinetic PCR and the application of standard curves," *Nucleic Acids Research,* vol. 31, p. e93, 2003.